

Novel Antagonist of the Type 2 Lysophosphatidic Acid Receptor (LPA₂), UCM-14216, Ameliorates Spinal Cord Injury in MiceNora Khiar-Fernández,[†] Debora Zian,[†] Henar Vázquez-Villa, R. Fernando Martínez, Andrea Escobar-Peña, Román Foronda-Sainz, Manisha Ray, Maria Puigdomenech-Poch, Giovanni Cincilla, Melchor Sánchez-Martínez, Yasuyuki Kihara, Jerold Chun, Rubèn López-Vales, María L. López-Rodríguez,* and Silvia Ortega-Gutiérrez*Cite This: *J. Med. Chem.* 2022, 65, 10956–10974

Read Online

ACCESS |



Metrics & More

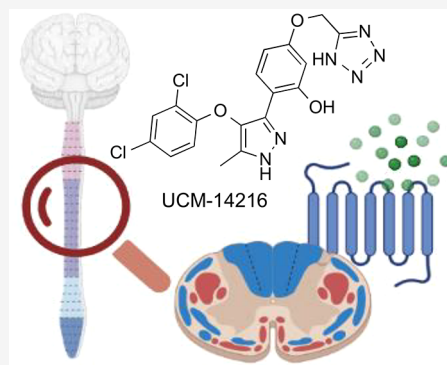


Article Recommendations



Supporting Information

ABSTRACT: Spinal cord injuries (SCIs) irreversibly disrupt spinal connectivity, leading to permanent neurological disabilities. Current medical treatments for reducing the secondary damage that follows the initial injury are limited to surgical decompression and anti-inflammatory drugs, so there is a pressing need for new therapeutic strategies. Inhibition of the type 2 lysophosphatidic acid receptor (LPA₂) has recently emerged as a new potential pharmacological approach to decrease SCI-associated damage. Toward validating this receptor as a target in SCI, we have developed a new series of LPA₂ antagonists, among which compound **54** (UCM-14216) stands out as a potent and selective LPA₂ receptor antagonist (E_{\max} = 90%, IC_{50} = 1.9 μ M, K_D = 1.3 nM; inactive at LPA_{1,3–6} receptors). This compound shows efficacy in an in vivo mouse model of SCI in an LPA₂-dependent manner, confirming the potential of LPA₂ inhibition for providing a new alternative for treating SCI.



INTRODUCTION

A spinal cord injury (SCI) is defined as damage to the spinal cord that provokes a temporary or permanent impairment of its function. It has negative consequences for the physical and social well-being of patients and imposes an important economic burden to the individual and the health care system. SCI can have traumatic or nontraumatic origins. The former happens when an external physical impact acutely harms the spinal cord, whereas the latter is associated with disease development, such as a tumor, an infection, or a neurodegenerative process. Regardless of the etiology, the primary injury damages cells and initiates a complex secondary cascade of secondary degeneration characterized by ischemia, excitotoxicity, and inflammatory processes that lead to the death of neurons and glial cells. This process is followed by a reorganization of the structural architecture of the spinal cord and by the formation of glial scars that, together with the poor capacity of the central nervous system (CNS) to promote remyelination and axonal growth, causes irreversible neurological deficits. Considering the negative impact of SCI, it is clear that prevention of the primary injury is desirable, as would an efficacious treatment to minimize secondary injury events to prevent functional impairments. The last several years have witnessed an important advancement of the field, with the development of different experimental neuroprotective and neuroregenerative therapies that have been translated from preclinical studies into clinical trials.^{1–3}

However, the current medical reality is that there is no treatment for acute SCI because methylprednisolone, which was the standard treatment for acute SCI, is no longer used for the management of spinal cord trauma in many countries based on several reports demonstrating its lack of therapeutic efficacy and its undesirable side effects related to immunosuppression and gastrointestinal bleeding.⁴ Hence, it is evident there is a crucial need to develop new treatments for SCI. In this regard, there is a consensus in that primary injury cannot be therapeutically addressed, but secondary cell damage events that occur after SCI could be susceptible to therapeutic intervention. Hence, much research effort has focused on delineation of the receptor pathways responsible for the irreversible cellular damage that occurs after SCI, because they could represent new therapeutic targets for novel drug treatments. In this context, bioactive lipids have recently emerged as major players in the initiation and maintenance of the pro-inflammatory environment that prevent tissue repair and recovery of homeostasis.⁵ Among them, lysophosphatidic acid (LPA, 1-acyl-*sn*-glycerol-3-phosphate) has received an

Received: January 11, 2022

Published: August 10, 2022



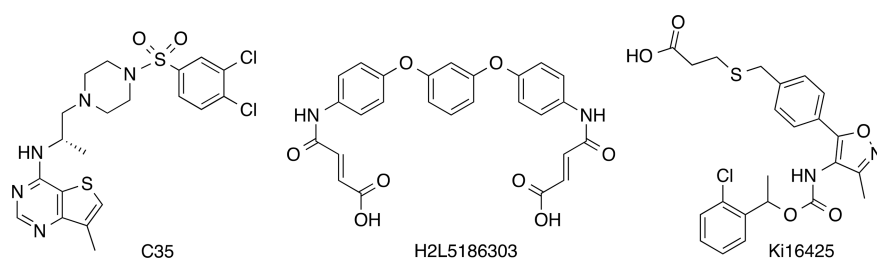


Figure 1. Structure of the LPA₂ antagonists C35, H2L5186303, and Ki16425.

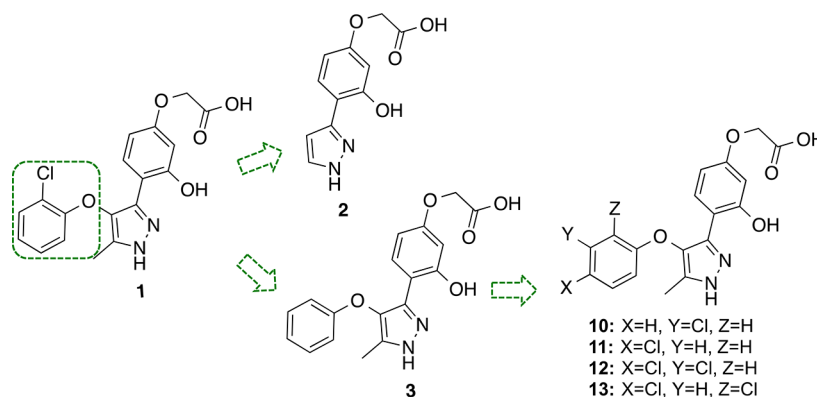


Figure 2. Design of new LPA₂ antagonists 2, 3, and 10–13.

increasing attention.^{6,7} Although LPA can refer to multiple different species of lysophospholipids with saturated (16:0, 18:0) and unsaturated (16:1, 18:1, 18:2, 20:4) acyl chains, in the context of SCI, LPA 18:1 (1-oleoyl-*sn*-glycerol-3-phosphate) appears to be the most important form.⁸ The increase in LPA levels in the CNS after traumatic injury has detrimental effects, as it has been confirmed by experiments showing that intraspinal injection of LPA leads to inflammation and demyelination.⁸ However, taking into account that LPA can activate at least six different receptors (LPA_{1–6}) that belong to the G protein-coupled receptor (GPCR) superfamily,^{9–11} the next important step is to determine which specific receptor subtype(s) is responsible for the deleterious effect of pathological LPA exposure. In this regard, the importance of LPA₁ as a target for the treatment of SCI has been well established,^{8,12} but this receptor does not account for all the effects observed with LPA. Very recently, LPA₂ has been postulated as a key receptor in mediating the effects of LPA in SCI.¹³ However, its validation has been hampered by the lack of selective antagonists. Currently, only two compounds (C35 and H2L5186303, Figure 1) have been characterized as potent (IC₅₀ values at LPA₂ of 0.017 and 0.0089 μM, respectively) and selective LPA₂ antagonists (IC₅₀ values >50 μM at LPA₁ and LPA₃ for C35 and 1.23 and 27.3 μM at LPA₁ and LPA₃ for H2L5186303).^{14,15} However, their selectivity profile versus the other LPA receptors (LPA_{4–6}), pharmacokinetic properties, and in vivo efficacy have not been studied. Another tool compound widely used to study the effect of blocking LPA receptor signaling is Ki16425 (Figure 1), but although it has good in vitro potency, this derivative is a nonselective antagonist with submicromolar activity at LPA₁ and LPA₃ and lower affinity at LPA₂ (IC₅₀ values of 0.34, 0.93, and 6.5 μM, respectively)¹⁶ and with limited in vivo activity that may reflect its short half-life.¹⁷

New potent and selective LPA₂ antagonists could enable the validation of this receptor as a target for the treatment of SCI

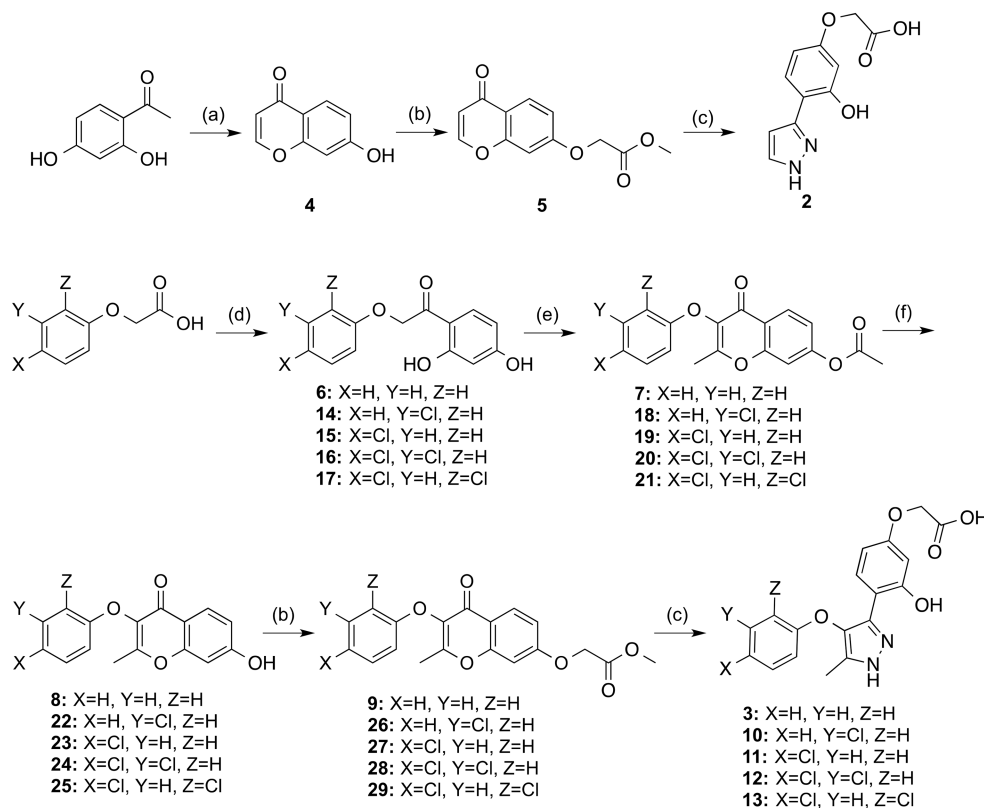
and might represent a new therapeutic avenue. Here we report the development of the most potent and selective LPA₂ antagonist described so far, compound UCM-14216 (**54**), which has an IC₅₀ value of 1.9 μM as an LPA₂ antagonist, a K_D value of 1.3 nM, and a selectivity over other LPA receptor subtypes (LPA₁ and LPA_{3–6}) with 10-fold selectivity in terms of IC₅₀ value with respect to LPA₁ and LPA₃ and 10-fold selectivity versus LPA₆ and >50-fold selectivity versus LPA₄ and LPA₅ in terms of K_D). In addition, this compound significantly improves motor recovery in an in vivo model of SCI, supporting the importance of LPA₂ for the treatment of SCI.

RESULTS AND DISCUSSION

Within a broad project focused on the discovery of new ligands for LPA receptors,¹⁸ we started our search of potent and selective LPA₂ antagonists through an in-house screen using a functional assay to detect calcium mobilization in cells stably transfected with the LPA₂ receptor in which the compounds under study were added at a fixed dose of 10 μM and the cells were subsequently stimulated with LPA at the same concentration. We considered active those compounds able to reduce the LPA-mediated calcium response by at least 30%. Among all tested molecules, compound **1** (Figure 2) showed a consistent antagonist signal at LPA₂ receptor, absence of significant agonist activity at this receptor (Figure S1), and selectivity versus LPA₁ and LPA₃ receptors, so it was selected as our initial hit. However, its moderate antagonism at LPA₂ at 10 μM ($E_{\max} = 48 \pm 9\%$) led us to carry out a systematic structural exploration of this compound with the aim of improving its biological activity.

Structure–Activity Relationship (SAR) Study of Hit 1.

First, we tried to establish the relative importance of the different parts of the molecule for the LPA₂ antagonist activity. We started by studying the influence of the chlorophenoxy

Scheme 1. Synthesis of Compounds 2, 3, and 10–13^a

^aReagents and conditions: (a) $\text{CH}(\text{OEt})_3$, 70% HClO_4 , H_2O , rt, 13 h, 47%; (b) methyl bromoacetate, K_2CO_3 , acetone, reflux, 3 h, 24–98%; (c) (i) 65% $\text{N}_2\text{H}_4 \cdot \text{H}_2\text{O}$, EtOH, reflux, 30 min, 77–99%; (ii) 2 M NaOH, EtOH, reflux, 12 h, 67–99%; (d) (i) SOCl_2 , toluene, 110 °C, 16 h, 99%; (ii) resorcinol, $\text{BF}_3 \cdot \text{Et}_2\text{O}$, DCM, reflux, 4–5 h, 19–25%; (e) acetic anhydride, Et_3N , NaOAc, 140 °C, 2–3 h, 83–99%; (f) conc. HCl, EtOH, reflux, 2 h, 75–99%.

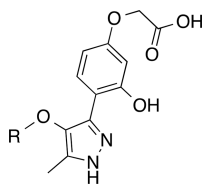
group by removing the whole moiety or just the halogen atom with the synthesis of compounds 2 and 3 (Figure 2).

Compound 2 was prepared from commercially available 1-(2,4-dihydroxyphenyl)ethanone by treatment with triethyl orthoformate and perchloric acid. Then, resulting hydroxychromone 4 was alkylated with methyl bromoacetate and treated with an excess of hydrazine to obtain desired derivative 2 (Scheme 1), through opening of the pyrone ring and subsequent formation of pyrazole ring. The reaction with hydrazine promoted the simultaneous transformation of the ester group to the corresponding hydrazide, which was hydrolyzed to obtain the target carboxylic acid. With respect to compound 3, its synthesis started with a Friedel–Crafts acylation between 2-phenoxyacetyl chloride and resorcinol. Next, the Kostanecki–Robinson reaction between the resulting ketone 6 and acetic anhydride afforded chromone 7 in a good yield, which was, after hydrolysis of the acetyl group in acid media, alkylated with methyl bromoacetate to obtain intermediate 9. Finally, treatment with hydrazine gave target compound 3 (Scheme 1). Antagonist activity assays revealed that compound 2 was inactive at LPA_2 ($E_{\text{max}} = 7 \pm 3\%$) whereas derivative 3 showed a low activity at LPA_2 ($E_{\text{max}} = 20 \pm 7\%$, Table 1), highlighting the need not only of the chlorine atom but also of the whole phenoxy system for the LPA_2 antagonist activity. Hence, we studied the influence of the position of the chloro substituent with the synthesis of compounds 10 and 11, where the chlorine atom was located in a meta or para position, respectively (Figure 2). These syntheses were accomplished following a synthetic route

similar to the one previously followed for compound 3 starting from the corresponding chlorophenoxyacetic acid and resorcinol (Scheme 1).

Determination of the LPA_2 antagonist character of compounds 10 and 11 revealed that whereas the former did not improve the antagonist activity of the initial hit 1 [E_{max} (1) = 48%; E_{max} (10) = 45%], the latter increased the LPA_2 antagonist activity at the maximum concentration [E_{max} (11) = 60%] (Table 1). These results suggested that the chlorine atom was tolerated at the three positions, with the best result obtained for the para derivative, so it may be possible that the introduction of a second chlorine atom allowed further improvement of activity. Accordingly, compounds 12 and 13 were synthesized (Scheme 1) and tested for LPA_2 activity (Table 1). Determination of their antagonist character revealed that introduction of the 2,4-dichlorophenoxy moiety yielded an excellent LPA_2 antagonist [E_{max} (13) = 84%; IC_{50} (13) = 5.5 μM ; Figure S2], with similar LPA_2 antagonist activity to Ki16425, used as the reference ligand (Table 1). Also, to rule out the existence of partial agonism, we measured the agonist activity of compounds 3 and 10–13 at LPA_2 receptors, and none of them was able to induce any significant activation of the receptor at 10 μM concentration (see Figure S1 for the result obtained for compound 13, which is representative of the rest of the compounds).

At this point, we considered that a detailed study of the molecular interactions involved in the affinity of compound 13 for LPA_2 could help us to rationalize the activity results and also shed some light on the binding site of the compound.

Table 1. Antagonist Activities of Compounds 1, 3, 10–13, and Ki16425 at LPA₁₋₃

Cpd	R	E_{\max} (%) ^a [IC ₅₀ (μM)] ^b		
		LPA ₁	LPA ₂	LPA ₃
1		N.E. ^c	48 ± 9	N.E.
3		N.E.	20 ± 7	N.E.
10		N.E.	45 ± 8	N.E.
11		N.E.	60 ± 9	N.E.
12		N.E.	58 ± 3	N.E.
13		N.E.	84 ± 3 [5.5 ± 0.7]	N.E.
Ki16425		97 ± 4 [0.8 ± 0.2]	92 ± 3 [1.2 ± 0.6]	99 ± 3 [1.6 ± 0.5]

^a E_{\max} = maximum blockade effect of the activation induced by 10 μM of LPA (18:1, 1-oleoyl-*sn*-glycerol-3-phosphate) at a concentration of the compound under study of 10 μM. ^bFor E_{\max} > 70%, IC₅₀ values are expressed as mean ± s.e.m, from a minimum of two independent experiments, performed in triplicate. ^cN.E., no effect was observed at the highest concentration of compound tested (10 μM).

Hence, we built a homology model of LPA₂ using the disclosed crystal structure of the LPA₁ as a template.¹⁹ The best docking pose of compound 13 in the LPA₂ receptor model (Figure 3A) suggests that the phenolic hydroxy group interacted with two hydrogen bonds with arginine 107 and glutamine 108 and the carboxylic acid group is engaged in two salt bridges with lysines 22 and 278 (Figure 3A). The dichlorophenoxy moiety lies in a hydrophobic pocket surrounded by leucine 261, leucine 111, glutamine 108, glycine 257, tryptophan 254, alanine 284, tyrosine 85 and phenylalanine 280. The chlorine atom in the 2-position points to residues leucine 111 and glutamine 108, while the one in the 4-position points to residues glycine 257 and alanine 284 (Figure 3A). Also, the oxygen atom of the phenoxy moiety forms a hydrogen bond with glutamine 108. Compound 3 adopts a similar pose to compound 13, but its phenoxy moiety does not completely fill the hydrophobic

pocket since it cannot simultaneously reach glycine 257, alanine 284, and leucine 111 as compound 13 does through its two chlorine atoms (Figure 3B).

The importance of the phenolic hydroxy group was confirmed through the synthesis of compound 30 (Scheme 2), which was obtained starting with a Williamson reaction between 2-bromo-1-(4-methoxyphenyl)ethanone and 2,4-dichlorophenol under microwave (MW) irradiation, using 1,8-diazabicyclo[5.4.0]undec-7-ene (DBU) as a base. Then, treatment of the intermediate 31 with 1,1-dimethoxy-*N,N*-dimethylethanamine yielded enaminone 32, which was reacted with hydrazine to obtain pyrazole 33. Finally, removal of the methoxy group followed by *O*-alkylation with methyl bromoacetate and hydrolysis of the ester gave the target pyrazole 30 (Scheme 2), which was basically inactive at the LPA₂ antagonist assay, with an E_{\max} value of only 11%.

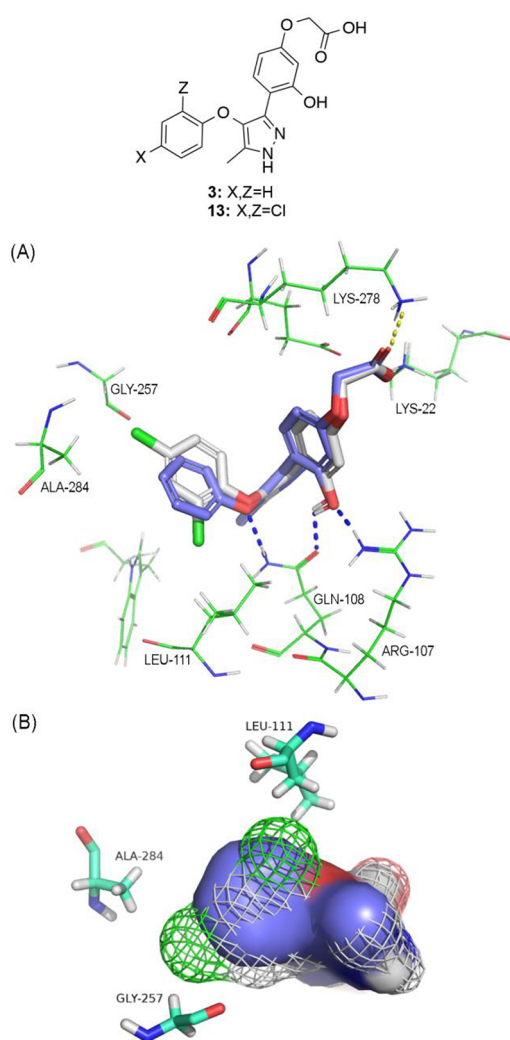


Figure 3. (A) LPA₁ (PDB ID 4Z35)-derived homology model of LPA₂R in complex with compounds 3 (in purple) and 13 (in white). The phenolic hydroxy group of both compounds is engaged in two hydrogen bonds with arginine 107 and glutamine 108 and the carboxylic acid group is engaged in two salt bridges with lysines 22 and 278. Also, the oxygen atom of the phenoxy moiety forms a hydrogen bond with glutamine 108. (B) Phenoxymoiety of the two compounds lies in the same hydrophobic pocket but compound 3, represented here with a C-purple surface representation, cannot reach simultaneously residues glycine 257, alanine 284, and leucine 111 as compound 13 does, represented here as C-white mesh representation.

Next, we focused our attention on the influence of the distance between the oxygen atom and the carboxylic acid group in compound 13. To determine the optimum length of the methylenic chain that separates these two moieties, we synthesized compounds 36–38, which have 2–4 methylenes in the linker (Scheme 3).

None of the synthesized compounds showed any activity as LPA₂ agonists at 10 μ M concentration and, in all cases, increasing the distance between the carboxylic acid group and the rest of the molecule resulted in decreased LPA₂ antagonism activity (Table 2). The worst result was obtained for compound 38, bearing the longest chain ($n = 4$) with an E_{\max} value of 21% compared to the 84% of derivative 13. This decrease in activity can be rationalized by the docking model between compound 38 and LPA₂ (Figure 4), which shows that a key salt bridge interaction between the carboxylic acid group

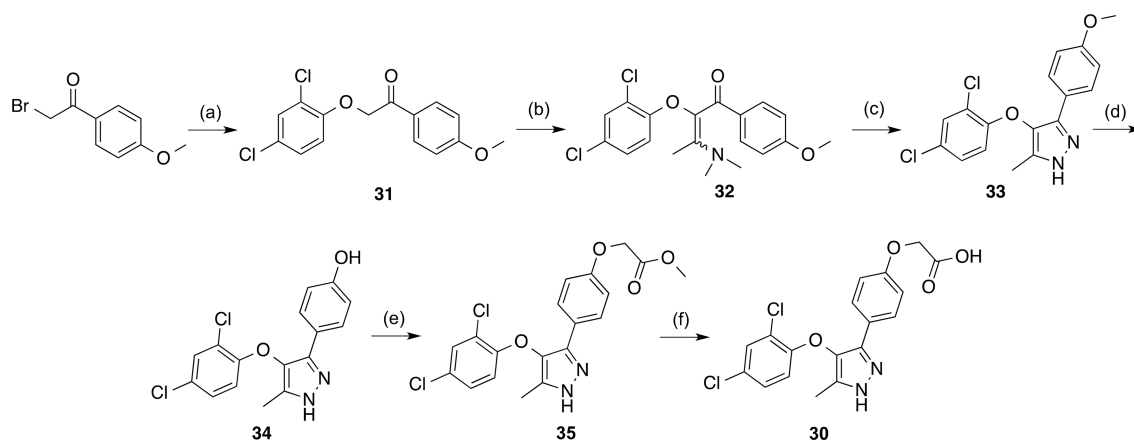
and lysine 22 can take place in compound 13 but not in derivative 38 due to the binding conformation induced by the four-unit spacer. In addition, a key hydrogen bond established between the phenolic hydroxy group of compound 13 and arginine 107 is missing in the binding of compound 38 to LPA₂ (Figure 4).

Further confirmation of the importance of the carboxylic acid interactions was obtained with the synthesis of compounds 42–45, where the carboxylic acid moiety was replaced by hydroxy, methoxy, methyl ester or carboxamide groups, respectively. The synthesis of these compounds started from chromone 25, which by reaction with hydrazine yielded pyrazole 42 that was further methylated to give 43. Alternatively, *O*-alkylation of chromone 25 with methyl bromoacetate or bromoacetamide followed by pyrazole ring formation yielded compounds 44 and 45 (Scheme 4). Biological evaluation of all these compounds (Table 3) revealed that only the methyl ester derivative 44 showed a good activity value ($E_{\max} = 74 \pm 7\%$; $IC_{50} = 11.6 \pm 0.4 \mu$ M). To further discard the existence of partial agonism, derivatives 42–45 were tested for their capacity to activate the LPA₂ receptor and none of them induced any appreciable effect at a concentration of 10 μ M.

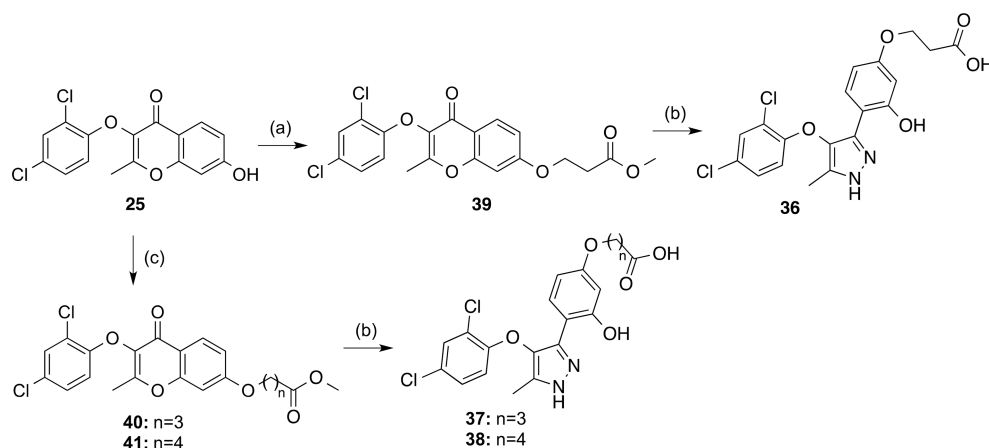
We next studied the effect of changes in the pyrazole ring. Specifically, we introduced an *N*-methyl group (compound 47), removed the methyl group located at position 5 of the heterocycle (compound 48), and replaced the pyrazole by an isoxazole ring (derivative 49). Direct methylation reaction of 13 provided *N*-methylated analogue 47 (Scheme 5), whereas the preparation of compound 48 started with the reaction of intermediate 17 with methanesulfonyl chloride, in the presence of the boron trifluoride diethyl etherate complex to obtain the corresponding hydroxychromone 50. Alkylation of this intermediate with ethyl bromoacetate and reaction with hydrazine, afforded desired pyrazole 48 (Scheme 5). Finally, isoxazole analogue 49 was obtained from chromone 29 using hydroxylamine (Scheme 5). Biological evaluation of the compounds (Table 4) revealed the importance of the methyl group in position 5 of the pyrazole ring for the antagonist activity, since derivative 48 exhibited a moderate E_{\max} value of 35%. With respect to derivatives 47 and 49, they showed good activity at LPA₂ but also a decrease in selectivity, since they display some antagonist character at LPA₃ (Table 4). None of them showed any activity as LPA₂ agonists at a concentration of 10 μ M.

In sum, these results indicated that derivative 13 was the best compound identified so far. Hence, we studied its pharmacokinetic profile. First, we estimated the membrane permeability using the parallel artificial membrane permeability assay (PAMPA) and its metabolic stability in mouse and human liver microsomes (MLMs and HLMs, respectively). In these assays, compound 13 showed a moderate permeability value (P) of 0.11×10^{-6} cm/s, considering as reference values $P < 1 \times 10^{-7}$ cm/s for low permeable compounds and $P > 1 \times 10^{-5}$ cm/s for highly permeable molecules. The metabolic stability was also moderate, with a half-life ($t_{1/2}$) of about 60 min in HLMs and 16 min in MLMs. Hence, it would be desirable to improve these parameters to obtain an optimized compound suitable for in vivo efficacy experiments.

Optimization of Compound 13. We initially addressed the optimization of derivative 13 with the replacement of chlorine atoms by fluorine in compound 53 (Scheme 6), as this change usually involves an improvement of the

Scheme 2. Synthesis of Compound 30^a

^aReagents and conditions: (a) 2,4-dichlorophenol, DBU, DMF, MW, 140 °C, 30 min, 80%; (b) 1,1-dimethoxy-*N,N*-dimethylethanamine, 90 °C, 4 h, 52%; (c) 65% $N_2H_4 \cdot H_2O$, EtOH, reflux, 1 h, 44%; (d) BBr_3 , DCM, -78 °C to rt, 21 h, 70%; (e) methyl bromoacetate, K_2CO_3 , DMF, -20 °C to rt, 16 h, 32%; (f) 1 M NaOH, 1,4-dioxane, 60 °C, 2 h, 99%.

Scheme 3. Synthesis of Compounds 36–38^a

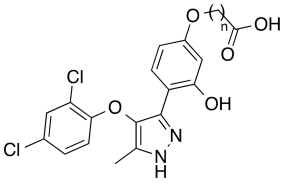
^aReagents and conditions: (a) methyl acrylate, DMAP, MW, 150 °C, 2.5 h, 10%; (b) (i) 65% $N_2H_4 \cdot H_2O$, EtOH, reflux, 30 min, 24–86%; (ii) 2 M NaOH, EtOH, reflux, 12 h, 86–99%; (c) methyl 4-bromobutanoate or methyl 5-bromopentanoate, K_2CO_3 , acetone, reflux, 3–5 h, 80–82%.

pharmacokinetic parameters.^{20,21} Also, considering that the free carboxylic acid could be responsible for the moderate permeability, it was replaced by the (bio)isostere tetrazole (compounds 54 and 55, Scheme 6). Tetrazole is among the most commonly employed carboxylic acid isosteres²² because its planarity and acidity closely resemble those of carboxylic acids ($pK_a = 4.5$ – 4.9). In addition, tetrazolate anions are more lipophilic than the corresponding carboxylates and they exhibit slightly different electrostatic potential and charge distribution due to the delocalization of the negative charge over the five-membered ring system. Then, synthesis of difluorinated derivative 53 was carried out following a similar route to the one described for compound 13 but starting with 2,4-difluorophenoxyacetic acid (Scheme 6). With respect to the tetrazole derivatives 54 and 55, they were prepared by alkylation of the intermediate chromones 25 and 58, respectively, with 2-bromoacetonitrile followed by sequential treatment with hydrazine and sodium azide to build the corresponding pyrazole and tetrazole rings, respectively (Scheme 6).

Biological evaluation of compounds 53–55 indicated that derivative 54 showed the best results, being the most potent

LPA₂ antagonist, with an E_{max} of 90% and an IC_{50} value of 1.9 μM (Figure S2), values that are superior to the ones showed by its analogue 13 (Table 5). None of these compounds showed any agonist activity at LPA₂ (see Figure S1 for the result obtained for compound 54, representative of the rest of the compounds).

Docking studies of these compounds showed how the docking pose of compound 54 is very similar to that of compound 13 by replacing the carboxylate moiety with its tetrazole ring (Figure 5A). In fact, the tetrazole moiety of compound 54 perfectly reproduces the interactions of the carboxylic acid of compound 13, substituting salt bridges for hydrogen bonds with lysines 22 and 278. With respect to the replacement of chlorine by fluorine in compounds 53 and 55, the dichloro and difluorophenoxy moieties lie in the same hydrophobic pocket (Figure 5B). However, the substitution of chlorine by fluorine atoms provokes a change in the orientation of the aromatic ring and hinders the difluorophenoxy moiety from simultaneously reaching residues leucine 111 and alanine 284 as observed for compounds 13 and 54 through their two chlorine atoms (Figures 3 and 5B). To experimentally validate the proposed docking model, we

Table 2. Antagonist activities of compounds 13, 36–38, and Ki16425 at LPA₁₋₃


compd	n	E_{\max} (%) ^a [IC ₅₀ (μM)] ^b		
		LPA ₁	LPA ₂	LPA ₃
13	1	N.E. ^c	84 ± 3 [5.5 ± 0.7]	N.E.
36	2	N.E.	67 ± 7	N.E.
37	3	N.E.	43 ± 12	N.E.
38	4	N.E.	21 ± 8	N.E.
Ki16425		97 ± 4 [0.8 ± 0.2]	92 ± 3 [1.2 ± 0.6]	99 ± 3 [1.6 ± 0.5]

^a E_{\max} = maximum blockade effect of the activation induced by 10 μM of LPA (18:1, 1-oleoyl-*sn*-glycerol-3-phosphate) at a concentration of the compound under study of 10 μM. ^bFor E_{\max} > 70%, IC₅₀ values are expressed as mean ± s.e.m, from a minimum of two independent experiments, performed in triplicate. ^cN.E., no effect was observed at the highest concentration of compound tested (10 μM).

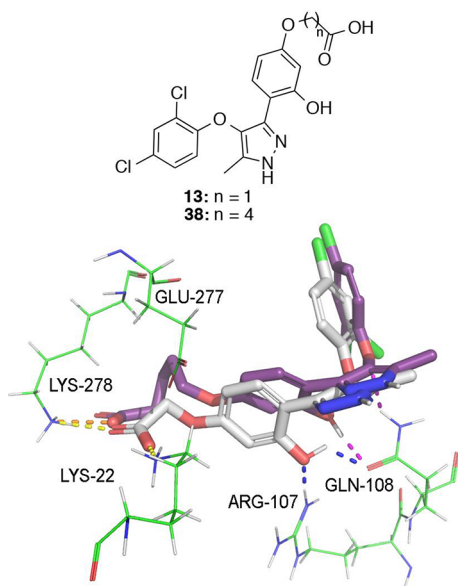


Figure 4. LPA₁ (PDB ID 4Z35)-derived homology model of LPA₂ in complex with compound 13 (in white) and compound 38 (in purple). Docking of compound 13 in the model suggests that the carboxylic acid of the compound is involved in two salt bridge interactions with lysine 22 and lysine 278; however, derivative 38 cannot form the salt bridge with lysine 22. Docking results also suggest that the phenolic hydroxy group of compound 13 establishes a hydrogen bond with arginine 107 and another one with glutamine 108, whereas derivative 38 can only establish hydrogen bonds with glutamine 108. For compound 13, salt bridges are colored in yellow and hydrogen bonds in blue, whereas for derivative 38, they are colored in orange and pink, respectively.

carried out point mutation experiments to confirm the importance of the most relevant residues (lysines 22 and 278, arginine 107, and glutamine 108). Thus, we transfected Mca-RH7777 cells with plasmids containing the corresponding N terminus HA-tagged LPA₂ mutant (K22A, R107A, Q108A, or K278A). Transfection efficacy was assessed by flow

cytometry using a primary antibody against HA and the appropriate fluorescent secondary antibody (Figure 6A) and the antagonist capacity of compound 54 was determined in cells transfected with each mutant. The obtained results indicate that replacement of any of the four amino acids (lysines 22 and 278, arginine 107 and glutamine 108) by alanine involved the lost of the antagonist activity of compound 54 (Figure 6B), thus confirming the importance of the proposed interactions. The data indicate that substitution of lysine 22, arginine 107, and glutamine 108 by alanine basically abolished the capacity of compound 54 to bind LPA₂ receptor (since no significant agonist nor antagonist activity was observed in the mutant receptors). However, the exchange of lysine 278 by alanine completely switched the functional activity of the receptor since compound 54 behaved as an agonist in this mutant receptor. Overall, these data suggest that amino acids 22, 107, and 108 are important for binding, whereas lysine 278 seems to be involved in the functional activity of the receptor.

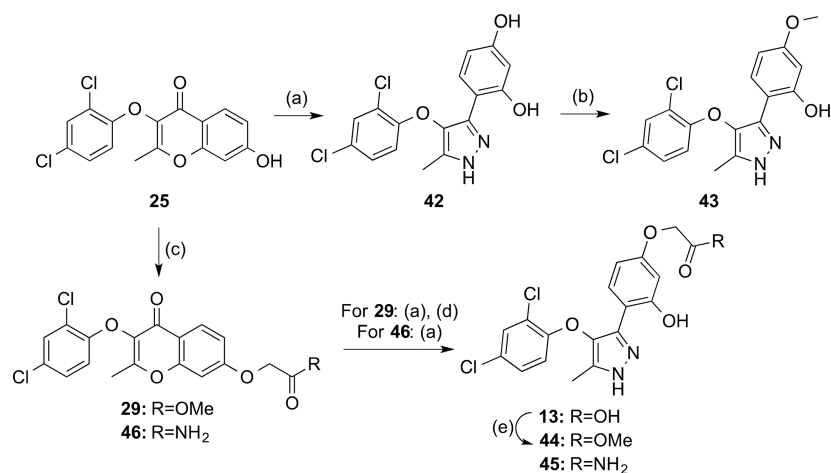
Noteworthy, compound 54 kept the receptor selectivity versus LPA₁ and LPA₃ (Table 5), so it emerged as an excellent candidate for in-depth pharmacological characterization.

In-Depth Characterization of Compound 54. First, we determined the membrane permeability using the PAMPA assay and the in vitro metabolic stability of the compound. The obtained results showed a good permeability value ($P = 6.1 \times 10^{-6}$ cm/s) and also increased stability in comparison with analog 13, with $t_{1/2}$ values of 50 ± 6 and 97 ± 15 min for MLMs and HLMs, respectively (Table 6).

These in vitro values correlated with the results obtained in the in vivo pharmacokinetic (PK) study, which was carried out to determine the suitability of the compound to reach the CNS in therapeutically relevant doses. For this aim, compound 54 was administered intraperitoneally (i.p.) at a dose of 25 mg/kg. Then, at different postinjection times (between 0.5 and 4 h), plasma, brain, and spinal cord samples were taken and the levels of compound 54 were measured using high-performance liquid chromatography coupled to mass spectrometry (HPLC-MS). These experiments confirmed the presence of compound 54 at significant levels in spinal cord and brain, with the maximum levels reached at one hour postadministration. These data (Table 7) indicate that antagonist 54 can readily cross the blood brain barrier and it is therefore an excellent candidate to validate the role of LPA₂ antagonism, at least as a proof of principle, in an in vivo model of SCI.

In addition, the binding affinity of the compound for LPA₂ was evaluated by means of a free solution assay-compensated interferometric reader (FSA-CIR) technique,^{23–26} showing a binding equilibrium constant (K_D) value of 1.3 nM. As a positive control, LPA showed a K_D value of 6.7 nM to LPA₂. The analogous assay carried out for LPA_{4–6} provided 10-fold selectivity versus LPA₆ and >50-fold selectivity versus LPA₄ and LPA₅ (Figure S3), making compound 54 (UCM-14216) the most potent and selective LPA₂ antagonist described so far.

In Vivo Efficacy Study of Compound 54 in an SCI Mouse Model. Since LPA₂ activation plays harmful actions after SCI, we finally assessed whether compound 54 protects against locomotor deficits in a spinal cord contusion injury model. It has been established that the LPA₂ receptor is constitutively expressed at very low levels in spinal cord and its transcripts are up-regulated during the first days after injury, returning to basal levels by day 7.¹³ This suggests that LPA-LPA₂ signaling in the injured spinal cord mainly occurs during

Scheme 4. Synthesis of Compounds 42–45^a

^aReagents and conditions: (a) 65% N₂H₄·H₂O, EtOH, reflux, 30 min, 65–80%; (b) CH₃I, K₂CO₃, acetone, 65 °C, 6 h, 20%; (c) methyl bromoacetate or bromoacetamide, K₂CO₃, acetone, reflux, 3 h, 51–67%; (d) 2 M NaOH, EtOH, reflux, 12 h, 90%; (e) CH₃OH, cat. H₂SO₄, reflux, 16 h, 85%.

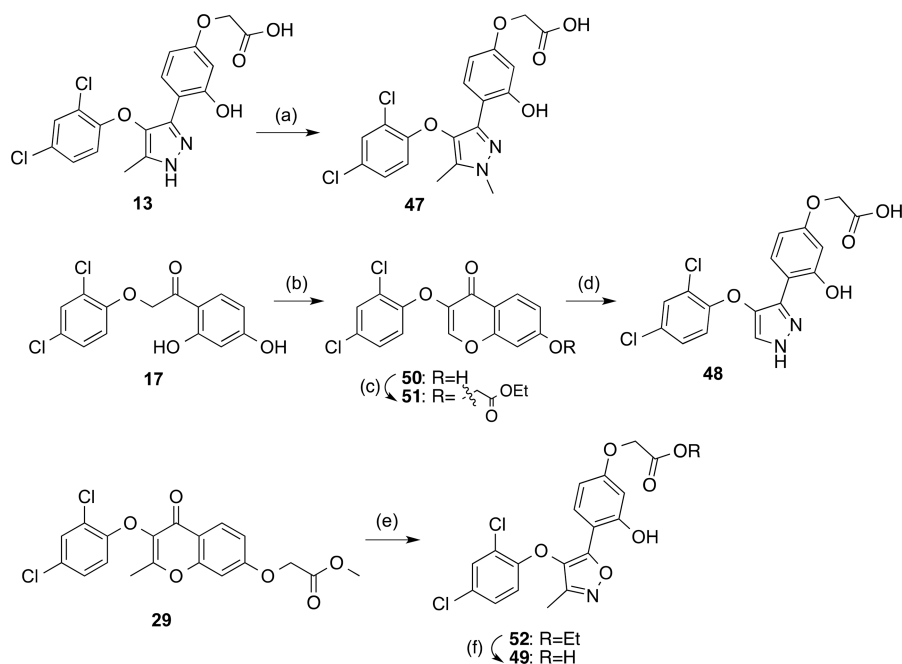
Table 3. Antagonist Activities of Compounds 13, 42–45, and Ki16425 at LPA₁₋₃

Cpd	R	E _{max} (%) ^a [IC ₅₀ (μM)] ^b		
		LPA ₁	LPA ₂	LPA ₃
13		N.E. ^c	84 ± 3 [5.5 ± 0.7]	N.E.
42	H	N.E.	16 ± 7	N.E.
43	Me	N.E.	9 ± 5	N.E.
44		N.E.	74 ± 7 [11.6 ± 0.4]	N.E.
45		N.E.	44 ± 7	N.E.
Ki16425		97 ± 4 [0.8 ± 0.2]	92 ± 3 [1.2 ± 0.6]	99 ± 3 [1.6 ± 0.5]

^aE_{max} = maximum blockade effect of the activation induced by 10 μM of LPA (18:1, 1-oleoyl-*sn*-glycerol-3-phosphate) at a concentration of the compound under study of 10 μM. ^bFor E_{max} > 70%, IC₅₀ values are expressed as mean ± s.e.m, from a minimum of two independent experiments, performed in triplicate. ^cN.E., no effect was observed at the highest concentration of compound tested (10 μM).

the first week postinjury. Hence, we hypothesized that administration of compound **54** for 10 days could block LPA-LPA₂ signaling in the injured spinal cord, and consequently, improve the outcome of SCI, as observed after genetic deletion of *Lpa₂*.¹³ The in vivo PK study suggested that an i.p. dose of 25 mg/kg was enough to reach significant levels of the compound one hour after administration (3.3 ng/mg tissue are equivalent approximately to a concentration of 2 μM in the spinal cord considering the volume of the sections used

in the study). It is conceivable that this concentration is even higher in the injured mice, as SCI results in increases permeability of the blood-spinal cord barrier.²⁷ Then, this dose was selected as the minimal capable of potentially eliciting the sought biological effects and simultaneously avoiding side effects related with the use of higher concentrations. Accordingly, mice were treated daily with compound **54** (25 mg/kg, i.p.) starting at 1 h following lesion and subsequently for 10 consecutive days, and locomotor performance was

Scheme 5. Synthesis of Compounds 47–49^a

^aReagents and conditions: (a) CH₃I, NaH, THF, rt, 16 h, 31%; (b) CH₃SO₂Cl, BF₃·Et₂O, DMF, 100 °C, 1.5 h, 94%; (c) ethyl bromoacetate, K₂CO₃, acetone, reflux, 3 h, 91%; (d) (i) 65% N₂H₄·H₂O, EtOH, reflux, 30 min, 99%; (ii) 2 M NaOH, EtOH, reflux, 12 h, 58%; (e) (i) NH₂OH·HCl, pyridine, EtOH, 85 °C, 12 h; (ii) *p*-toluenesulfonic acid, EtOH, 78 °C, 5 h, 40%; (f) 1 M NaOH, 1,4-dioxane, 60 °C, 16 h, 91%.

Table 4. Antagonist Activities of Compounds 13, 47–49, and Ki16425 at LPA₁₋₃

compd	R	R'	X	E_{\max} (%) ^a [IC ₅₀ (μM)] ^b		
				LPA ₁	LPA ₂	LPA ₃
13	Me	H	N	N.E. ^c	84 ± 3 [5.5 ± 0.7]	N.E.
47	Me	Me	N	N.E.	73 ± 10	47 ± 7
48	H	H	N	N.E.	35 ± 8	N.E.
49	Me	H	O	N.E.	58 ± 3	71 ± 4
Ki16425				97 ± 4 [0.8 ± 0.2]	92 ± 3 [1.2 ± 0.6]	99 ± 3 [1.6 ± 0.5]

^a E_{\max} = maximum blockade effect of the activation induced by 10 μM LPA (18:1, 1-oleoyl-*sn*-glycerol-3-phosphate) at a concentration of the compound under study of 10 μM. ^bFor E_{\max} > 70% and selectivity at LPA₂ receptor, IC₅₀ values are expressed as mean ± s.e.m, from a minimum of two independent experiments, performed in triplicate. ^cN.E., no effect was observed at the highest concentration of compound tested (10 μM).

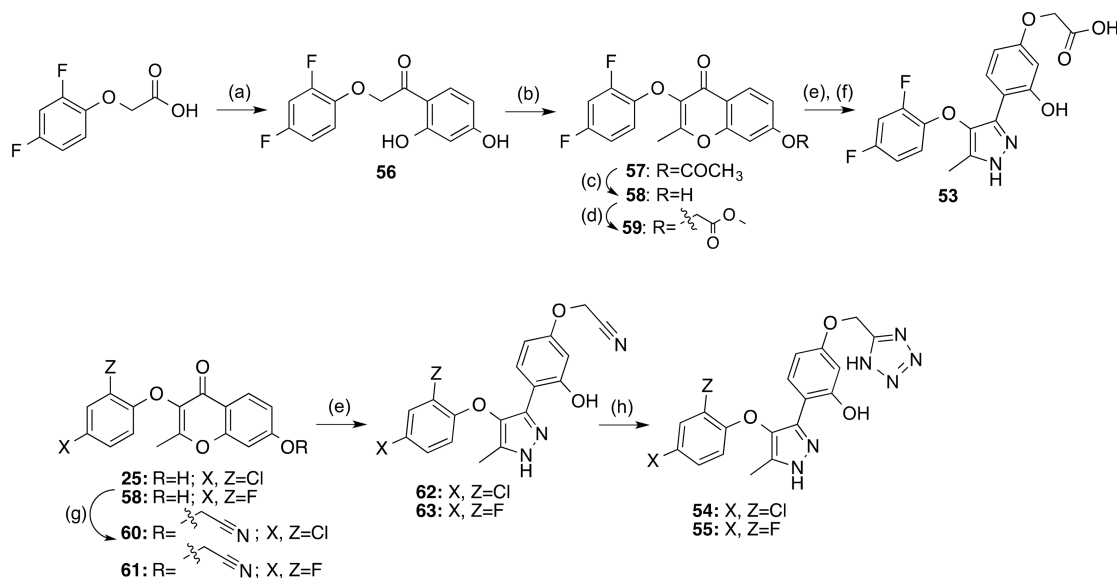
assessed by using the Basso Mouse Scale (BMS). BMS is the gold standard test used for locomotor scoring after SCI in which two blinder observers score the mouse motor performance based on a nine-point scale.²⁸ As shown in Figure 7A, mice treated with compound 54 displayed significant improvement in locomotor recovery after SCI. Bonferroni's post hoc analysis revealed that motor skills were significantly enhanced in the injured mice that had been treated with compound 54 for 10 days at 25 mg/kg, from day 35 postinjury onward. At the end of the follow up (day 50 postinjury) mice treated with vehicle showed plantar placement of the hind paw but no weight-bearing stepping (BMS score 3.0 ± 0.2). In contrast, mice treated with compound 54 displayed occasional or frequent stepping (BMS of 4.1 ± 0.3). We do not discard that the therapeutic actions of the compound 54 could be enhanced

with more frequent administration (i.e., twice a day), longer duration or greater dose of the compound.

Importantly, the observed locomotor improvement is largely mediated by the action of the compound at the LPA₂ receptor, because administration of the same dose of compound to LPA₂ null mice undergoing SCI did not induce any significant effect (Figure 7B). These results clearly validate the LPA₂ receptor as a valuable therapeutic target for the treatment of SCI.

CONCLUSIONS

In this work, we report the synthesis of the most potent and selective LPA₂ antagonist identified to date, compound 54 (UCM-14216), with functional E_{\max} and IC₅₀ values of 90% and 1.9 μM, respectively, and a K_D value of 1.3 nM at LPA₂ and functional selectivity against other LPA receptors

Scheme 6. Synthesis of Compounds 53–55^a

^aReagents and conditions: (a) (i) SOCl₂, toluene, 110 °C, 16 h, 99%; (ii) resorcinol, BF₃·Et₂O, DCM, reflux, 4 h, 10%; (b) acetic anhydride, Et₃N, NaOAc, 140 °C, 2.5 h, 71%; (c) conc. HCl, EtOH, reflux, 2 h, 99%; (d) methyl bromoacetate, K₂CO₃, acetone, reflux, 3 h, 99%; (e) 65% N₂H₄·H₂O, EtOH, reflux, 30 min, 21–99%; (f) 2 M NaOH, EtOH, reflux, 12 h, 61%; (g) bromoacetonitrile, K₂CO₃, acetone, reflux, 3–5 h, 77–93%; (h) NaN₃, NH₄Cl, DMF, reflux, 16 h, 52–72%.

Table 5. Antagonist Activities of Compounds 13, 53–55, and Ki16425 at LPA₁₋₃

Cpd	X, Z	R	E _{max} (%) ^a [IC ₅₀ (μM)] ^b		
			LPA ₁	LPA ₂	LPA ₃
13	Cl	COOH	N.E. ^c	84 ± 3 [5.5 ± 0.7]	N.E.
53	F	COOH	N.E.	65 ± 11 [5.1 ± 0.1]	N.E.
54	Cl		N.E.	90 ± 2 [1.9 ± 0.2]	N.E.
55	F		N.E.	77 ± 5 [31 ± 12]	N.E.
Ki16425			97 ± 4 [0.8 ± 0.2]	92 ± 3 [1.2 ± 0.6]	99 ± 3 [1.6 ± 0.5]

^aE_{max} = maximum blockade effect of the activation induced by 10 μM of LPA (18:1, 1-oleoyl-*sn*-glycerol-3-phosphate) at a concentration of the compound under study of 10 μM. ^bFor E_{max} > 60%, IC₅₀ values are expressed as mean ± s.e.m, from a minimum of two independent experiments, performed in triplicate. ^cN.E., no effect was observed at the highest concentration of compound tested (10 μM).

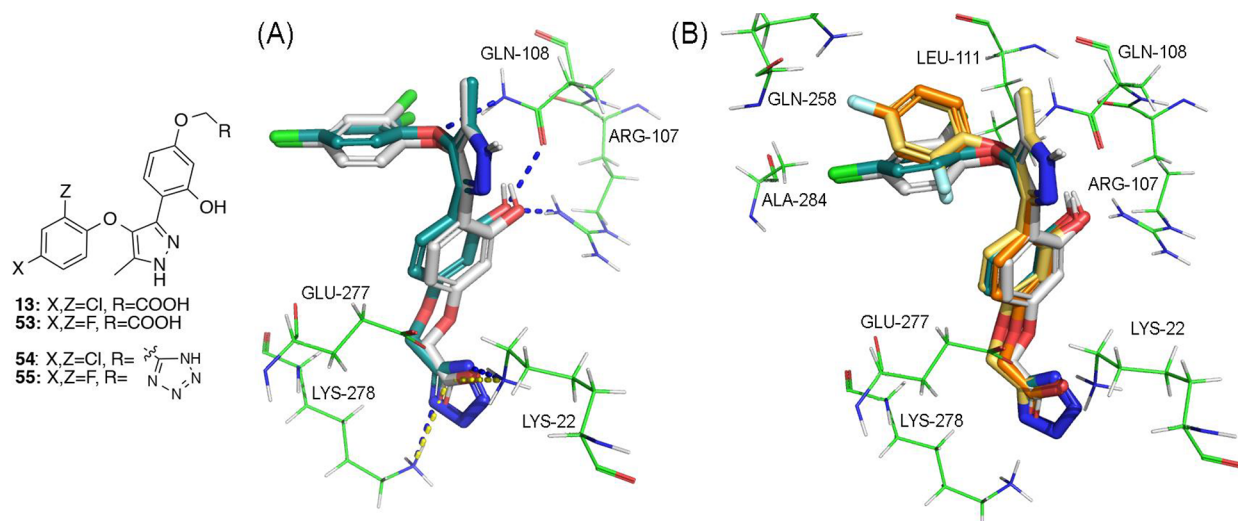


Figure 5. (A) LPA₁ (PDB ID 4Z35)-derived homology model of LPA₂ in complex with compounds 13 (in white) and 54 (in turquoise). The tetrazole moiety of compound 54 interacts in a similar manner to the carboxylic acid group of compound 13. Thus, the carboxylic acid forms salt bridges with lysines 22 and 278 (in yellow) and the tetrazole ring establishes hydrogen bonds with these two residues (in blue). The rest key interactions are maintained in both compounds. (B) LPA₁-derived homology model of LPA₂ in complex with compounds 13 (in white), 53 (in orange), 54 (in turquoise), and 55 (in yellow). The dichlorophenoxy and difluorophenoxy moieties of compounds 13 and 53–55 lie in the same hydrophobic pocket. However, the substitution of chlorine for fluorine provokes a change in the orientation of the aromatic ring and prevents compounds 53 and 55 from reaching residues leucine 111 and alanine 284.

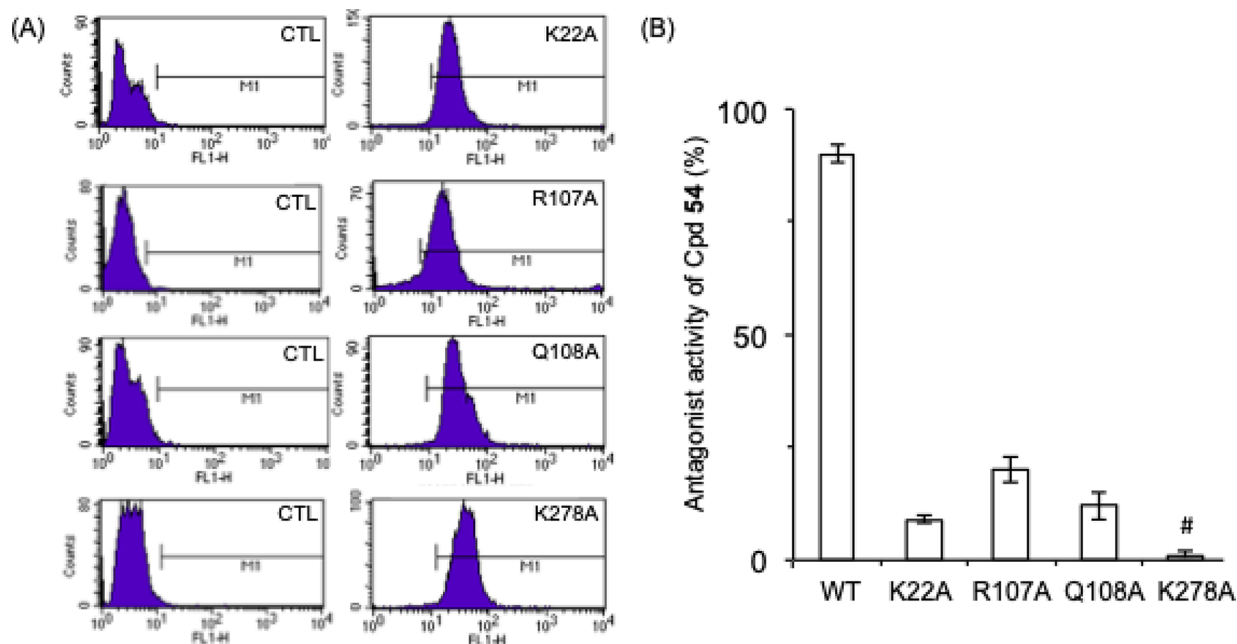


Figure 6. (A) Cell surface expression of each mutant LPA₂ receptor was assessed by flow cytometry using an anti-HA antibody raised in mice followed by an antimouse antibody conjugated to Alexa 488 in McA-RH7777 cells transiently transfected with mock plasmid (CTL, control) or with plasmids containing the indicated LPA₂ mutant receptor. (B) Capacity of compound 54 (10 μ M) to block the activation induced by 10 μ M of LPA (18:1, 1-oleoyl-*sn*-glycerol-3-phosphate) in the indicated mutant LPA₂ receptor. Values are expressed as mean \pm s.e.m, from two independent experiments performed in triplicate. Values obtained for the four point mutations have differences statistically significant ($p < 0.01$) with respect to the value obtained for the wild type (WT) receptor. #Compound 54 behaved as an agonist of the LPA₂ K278A mutant (able to induce 75 \pm 5% activation at 10 μ M, being the stimulation produced by 10 μ M LPA normalized to 100%).

(LPA_{1,3-6}). In addition, compound 54 has a good pharmacokinetic profile both in vitro and in vivo, reaching pharmacologically relevant levels in the CNS, where the site of action is located. Furthermore, it shows efficacy in an acute in vivo mouse model of SCI being inactive in LPA₂ knockout mice undergoing the same model, thus supporting the involvement of LPA₂ in the secondary damage that follows

SCI. SCI mainly affects to young and otherwise healthy adults, who suffer from a lack of efficacious treatments. Current treatments are generally palliative, limited to analgesic and anti-inflammatory drugs, underscoring high medical need for new pharmacological strategies that might be accessed by LPA₂ antagonists to ameliorate SCI pathophysiology and improve neurological outcomes. Further study of UCM-14216 and

Table 6. In Vitro Pharmacokinetic Profile of Compounds 13 and 54

compd	stability ($t_{1/2}$, min) ^a		P (cm/s) ^b	clogP ^c
	MLMs	HLMs		
13	16 ± 8	61 ± 10	0.1 × 10 ⁻⁶	4.14
54	50 ± 6	97 ± 15	6.1 × 10 ⁻⁶	3.29

^aData for stability in mouse and human liver microsomes (MLMs and HLMs, respectively) are expressed as the mean ± s.e.m. from five independent experiments performed in duplicate. ^b P = permeability value; reference values consider $P < 10^{-7}$ cm/s for low permeability compounds and $P > 10^{-5}$ cm/s for highly permeable molecules. ^cValues obtained with the ACDLabs *Percepta* software (version 6.0).

Table 7. In Vivo Levels of Compound 54 at Different Post-injection Times

sample	concentration of compound 54 (ng/mg tissue) after the indicated postinjection time (h) ^a			
	0.5	1	2	4
plasma	130 ± 50	41 ± 5	38 ± 1	ND
spinal cord	0.40 ± 0.06	3.3 ± 0.3	ND ^b	ND
brain	0.10 ± 0.02	28 ± 4	0.08 ± 0.01	ND

^aMice received a single injection of compound 54 (25 mg/kg, i.p.). Samples were taken at the indicated postinjection times and immediately frozen, and the levels of compound were then analyzed by HPLC-MS. Data are the means ± s.e.m. from three independent samples. ^bND, not detected.

other related compounds could provide novel approaches to treat SCI and possibly other traumatic CNS injuries.

EXPERIMENTAL SECTION

Synthesis. Unless stated otherwise, starting materials, reagents, and solvents were purchased as high-grade commercial products from Sigma-Aldrich, Alfa Aesar, Acros, Fluka, Panreac or Scharlab, and were used without further purification. Dichloromethane (DCM) and tetrahydrofuran (THF) were dried using a Pure Solv Micro 100 Liter solvent purification system. Triethylamine and pyridine were dried over KOH and distilled prior to its use. All nonaqueous reactions were performed under an argon atmosphere in oven-dried glassware unless otherwise stated. MW irradiation reactions were carried out on a Biotage Initiator 2.5 reactor, using Biotage vials sealed with an aluminum/Teflon crimp top, which can be exposed to a maximum of 250 °C and 20 bar internal pressure.

Analytical thin-layer chromatography (TLC) was run on Supelco silica gel plates (silica gel 60 F₂₅₄) with detection by UV light (254 nm) and 5% ninhydrin solution in ethanol or 10% phosphomolybdic acid solution in ethanol. Products were purified by flash chromatography on glass columns using silica gel (60 Å pore size, 230–400 mesh particle size from Supelco) or using a Varian 971-FP system with cartridges of silica gel (Varian, 50 μm size particle).

All compounds were obtained as oils, except for those whose melting points (mp) are indicated, which were solids. Mp values were determined on a Stuart Scientific electrothermal apparatus. Infrared (IR) spectra were measured on a Bruker Tensor 27 instrument equipped with a Specac ATR accessory of 5200–650 cm⁻¹ transmission range; frequencies (ν) are expressed in cm⁻¹.

Nuclear magnetic resonance (NMR) spectra were recorded at rt on a Bruker Avance III 700 MHz (¹H, 700 MHz; ¹³C, 175 MHz), Bruker Avance 500 MHz (¹H, 500 MHz; ¹³C, 125 MHz) or Bruker DPX 300 MHz (¹H, 300 MHz; ¹³C, 75 MHz) instrument at the Universidad Complutense de Madrid (UCM) NMR core facility. ¹⁹F-NMR spectra were recorded on a Bruker DPX 300 MHz. Chemical shifts (δ) are expressed in parts per million relative to the residual solvent peak for ¹H and ¹³C nucleus (CDCl₃: $\delta_H = 7.26$, $\delta_C = 77.2$; MeOH-*d*₄: $\delta_H = 3.31$, $\delta_C = 49.0$; DMSO-*d*₆: $\delta_H = 2.50$, $\delta_C = 39.5$), and coupling constants (J) are in hertz (Hz). The following abbreviations are used to describe peak patterns when appropriate: s (singlet), d (doublet), t (triplet), q (quadruplet), m (multiplet), br (broad), and app (apparent). 2D NMR experiments (COSY, HMQC, and HMBC) of representative compounds were carried out to assign protons and carbons of new structures; for those carbons displaying very broad signals in ¹³C NMR spectra, the corresponding chemical shifts were established by their correlation peaks in HSQC and HMBC spectra (Figure S4 shows the numbered structures used in the structural characterization by NMR of all final compounds). High-resolution mass spectrometry (HRMS) was carried out on a FTMS Bruker APEX Q IV spectrometer in electrospray ionization (ESI) or matrix-assisted laser desorption ionization (MALDI) mode at UCM's mass spectrometry facilities.

For all final compounds, purity was determined by HPLC-MS and satisfactory chromatograms confirmed a purity of at least 95%. HPLC-MS analysis was performed using an Agilent 1200LC-MSD VL instrument. LC separation was achieved with an Eclipse XDB-C₁₈ (5 μm, 4.6 mm × 150 mm) or a Zorbax SB-C₃ column (5 μm, 2.1 mm × 50.0 mm) together with a guard column (5 μm, 4.6 mm × 12.5 mm). Mobile phase consisted of A (95:5 water/acetonitrile) and B (5:95 water/acetonitrile) with 0.1% formic acid as solvent modifier. Gradients are indicated in Table S1. MS analysis was performed with an ESI source. The capillary voltage was set to 3.0 kV and the fragmentor voltage was set at 72 eV. The drying gas temperature was 350 °C, the drying gas flow was 10 L/min, and the nebulizer pressure

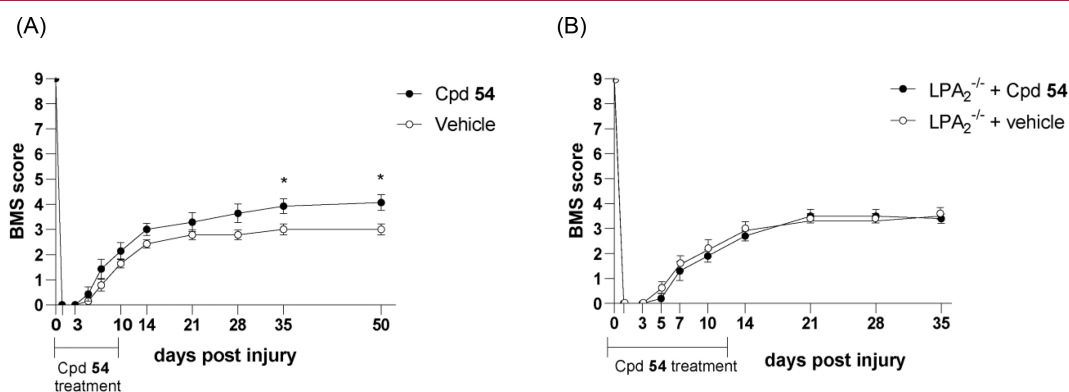


Figure 7. Compound 54 significantly improves locomotor recovery after SCI in LPA₂ wild type mice but not in LPA₂ deficient mice. Effect of i.p. injection of 54 (25 mg/kg) or vehicle on locomotor recovery in (A) C57bl/6 mice and (B) LPA₂ deficient mice quantified using the 0 (absence of movement) to 9 (completely normal locomotor behavior) Basso Mouse Scale (BMS). Data are expressed as mean ± s.e.m. and correspond to seven animals per group in A and five animals per group in B. * $p < 0.05$ compared with vehicle-treated group (two-way repeated measures ANOVA with Bonferroni's post hoc test for multiple comparisons).

was 20 psi. Spectra were acquired in positive or negative ionization mode from 100 to 1000 m/z and in UV-mode at four different wavelengths (210, 230, 254, and 280 nm).

General Procedure 1: Friedel–Crafts Acylation. (a) Preparation of the aryloxyacetyl chloride: to a solution of the corresponding aryloxyacetic acid (1 equiv.) in anhydrous toluene (5.5 mL/mmol) was added thionyl chloride (2.8 mL/mmol) and the reaction mixture was refluxed for 16 h. After this time, the excess of thionyl chloride and toluene were evaporated under reduced pressure, affording the corresponding aryloxyacetyl chloride in quantitative yield. (b) Friedel–Crafts acylation: to a cooled (0 °C) stirred solution of the corresponding freshly prepared aryloxyacetyl chloride (1 equiv.) and resorcinol (1.1 equiv.) in anhydrous DCM (1.5 mL/mmol), boron trifluoride diethyl etherate (1.3 mL/mmol) was added. The reaction was stirred at 0 °C for 10 min and then at 90 °C until starting material was consumed (TLC, 4–5 h). The reaction vessel was then cooled in an ice bath and the mixture poured into an excess of ice water. The aqueous phase was extracted with DCM (×2), and the combined organic layers were washed with brine, dried over Na_2SO_4 , filtered and concentrated under reduced pressure. The residue was purified by flash chromatography to yield the corresponding 2,4-dihydroxyphenylethanones **6**, **14–17**, and **56**.

General Procedure 2: Synthesis of Chromones by Kostanecki–Robinson Acylation. A mixture of the corresponding 2,4-dihydroxyphenylethanone (1 equiv.), freshly distilled acetic anhydride (0.6 mL/mmol), triethylamine (0.8 mL/mmol), and anhydrous sodium acetate (2.4 equiv.) was stirred at 140 °C until the reaction was completed (TLC, 2–3 h). Afterward, cold water was added and the mixture was extracted with DCM (×2). The combined organic phases were washed with brine, dried over Na_2SO_4 , filtered, and concentrated under reduced pressure, affording the corresponding acetoxychromones **7**, **18–21**, and **57**, which were used without further purification.

General Procedure 3: Hydrolysis of Acetoxychromone Derivatives. To a solution of the appropriate acetoxychromone (1 equiv.) in the minimum amount of absolute ethanol was added conc. HCl (0.6 mL/mmol), and the reaction was refluxed for 2 h. After cooling to rt, the mixture was diluted with ethyl acetate and washed with a saturated aqueous solution of NaHCO_3 and brine. The organic phase was dried over Na_2SO_4 , filtered, and concentrated under reduced pressure, affording the corresponding hydroxychromones **8**, **22–25**, and **58**, which were used without further purification.

General Procedure 4: Alkylation of Hydroxychromone Derivatives. To a solution of the corresponding hydroxychromone (1 equiv.) in anhydrous acetone (15 mL/mmol) was added K_2CO_3 (2 equiv), and the reaction mixture was refluxed for 30 min. Then, a solution of the appropriate bromoderivative (1.1–4.3 equiv.) in anhydrous acetone (1 mL/mmol) was added and the mixture was refluxed until consumption of starting material (TLC, 3–5 h). Next, cold water was added and acetone was removed under reduced pressure. The aqueous residue was extracted with DCM (×2), and the combined organic phases were washed with brine, dried with Na_2SO_4 , filtered, and concentrated under reduced pressure. The residue was purified by flash chromatography to afford the corresponding alkylated chromones **5**, **9**, **26–29**, **40**, **41**, **46**, **51**, **59**, **60**, and **61**.

General Procedure 5: Synthesis of Pyrazole Derivatives by Reaction with Hydrazine. A solution of the corresponding chromone or enamionone (1 equiv.) in absolute ethanol (5 mL/mmol) at 40 °C was treated with a solution of hydrazine monohydrate (65%, 0.18 mL/mmol) in absolute ethanol (1.3 mL/mmol), and the mixture was refluxed until the reaction was completed (TLC, 0.5–2 h). After cooling to rt, the mixture was concentrated under reduced pressure and the residue was dissolved with ethyl acetate and acidified with 1 M HCl until pH 6. The aqueous phase was extracted with ethyl acetate (×2), and the combined organic layers were washed with brine, dried over Na_2SO_4 , filtered, and concentrated under reduced pressure. The residue was purified by flash chromatography to yield the corresponding pure pyrazoles **33**, **42**, **45**, **62**, and **63**. For those chromones or enamionones bearing an ester group, the resulting

hydrazide derivative was taken to next step (General Procedure 6) without further purification.

General Procedure 6: Hydrolysis of Hydrazide Derivatives. To a solution of the corresponding hydrazide obtained according to General Procedure 5 (1 equiv.) in the minimum amount of 96% ethanol was added 2 M NaOH (0.8 mL/mmol), and the reaction was refluxed for 12 h. After cooling to rt, the mixture was diluted with ethyl acetate and acidified with 1 M HCl until pH 6. The aqueous phase was extracted with ethyl acetate (×2) and the combined organic layers were washed with brine, dried over Na_2SO_4 , filtered, and concentrated under reduced pressure. The residue was purified by flash chromatography to yield target carboxylic acid derivatives **2**, **3**, **10–13**, **36–38**, **48**, and **53**.

General Procedure 7: Synthesis of Tetrazole Derivatives. To a solution of the corresponding nitrile (1 equiv.) in anhydrous DMF (15 mL/mmol), NH_4Cl (1.5 equiv.), and NaN_3 (1.5 equiv.) were added, and the reaction was refluxed overnight. Then, the mixture was filtered to remove salts, and the resulting solution was acidified until pH 3 with 1 M HCl and extracted with ethyl acetate (×2). The combined organic phases were washed with a 1:1 mixture of water/brine, dried with Na_2SO_4 , filtered, and concentrated under reduced pressure. The residue was purified by flash chromatography to afford the corresponding tetrazoles **54** and **55**.

[3-Hydroxy-4-(1H-pyrazol-3-yl)phenoxy]acetic Acid (2). Following general procedures 5 and 6, pyrazole **2** was obtained from chromone **5** (29 mg, 0.12 mmol) in 98% yield. Chromatography: DCM to DCM/methanol, 8:2. Mp: 92–94 °C. R_f : 0.79 (DCM/methanol, 7:3). IR (ATR): ν 3404 (OH, NH); 1623 (C=O). ^1H NMR (DMSO- d_6 , 700 MHz): δ 4.35 (s, 2H, CH_2); 6.41–6.43 (m, 2H, H_2 , H_6); 6.71 (br s, 1H, H_4); 7.56 (d, $J = 8.7$, 1H, H_5); 7.80 (br s, 1H, H_5); 11.05 (br s, 1H, OH); 13.13 (br s, 1H, NH). ^{13}C NMR (DMSO- d_6 , 175 MHz): δ 66.6 (CH_2); 101.3 (C_4); 102.0 (C_2); 106.3 (C_6); 110.0 (C_4); 127.3 (C_5); 130.0 (C_5); 150.3 (C_3); 156.3 (C_3); 159.1 (C_1); 171.5 (C=O). HRMS (ESI, m/z): calcd for $\text{C}_{11}\text{H}_9\text{N}_2\text{O}_4$ [M-H] $^-$: 233.0568; found: 233.0559. HPLC (method B, t_R , min): 10.97.

[3-Hydroxy-4-(5-methyl-4-phenoxy-1H-pyrazol-3-yl)phenoxy]acetic Acid (3). Following general procedures 5 and 6, pyrazole **3** was obtained from chromone **9** (10 mg, 0.03 mmol) in 99% yield. Chromatography: DCM to DCM/methanol, 7:3. Mp: >180 °C (decomp.). R_f : 0.92 (DCM/methanol, 7:3). IR (ATR): ν 3440 (OH, NH); 1636 (C=O). ^1H NMR (methanol- d_4 , 700 MHz): δ 2.11 (s, 3H, CH_3); 4.38 (s, 2H, CH_2); 6.32 (dd, $J = 8.7$, 2.2, 1H, H_6); 6.46 (d, $J = 2.2$, 1H, H_2); 6.88–6.91 (m, 2H, H_2 , H_6); 6.99 (t, $J = 7.4$, 1H, H_4); 7.26–7.29 (m, 2H, H_3 , H_5); 7.56 (d, $J = 8.8$, 1H, H_5). ^{13}C NMR (methanol- d_4 , 175 MHz): δ 8.8 (CH_3); 67.9 (CH_2); 103.3 (C_2); 107.0 (C_6); 110.6 (C_4); 115.9 (C_2 , C_6); 123.2 (C_4); 128.7 (C_5); 130.8 (C_3 , C_5); 133.6 (C_4 , C_5); 159.7 (C_3); 160.6 (C_1 , C_1); 177.2 (C=O); C_3 , not observed. HRMS (ESI, m/z): calcd for $\text{C}_{18}\text{H}_{15}\text{N}_2\text{O}_5$ [M-H] $^-$: 339.0986; found: 339.0975. HPLC (method B, t_R , min): 21.34.

[4-[4-(3-Chlorophenoxy)-5-methyl-1H-pyrazol-3-yl]-3-hydroxyphenoxy]acetic Acid (10). Following the general procedures 5 and 6, pyrazole **10** was obtained from chromone **26** (49 mg, 0.64 mmol) in 67% yield. Chromatography: ethyl acetate to ethyl acetate/methanol, 8:2. Mp: >240 °C (decomp.). R_f : 0.18 (ethyl acetate/methanol, 8:2). IR (ATR): ν 3346 (OH, NH); 1585 (C=O). ^1H NMR (methanol- d_4 , 700 MHz): δ 2.12 (s, 3H, CH_3); 4.42 (s, 2H, CH_2); 6.35 (dd, $J = 8.8$, 2.5, 1H, H_6); 6.47 (d, $J = 2.5$, 1H, H_2); 6.83 (ddd, $J = 8.4$, 2.3, 0.6, 1H, H_6); 6.90 (t, $J = 2.2$, 1H, H_2); 7.00 (dd, $J = 7.9$, 1.5, 1H, H_4); 7.25 (t, $J = 8.2$, 1H, H_5); 7.50 (d, $J = 8.7$, 1H, H_5). ^{13}C NMR (methanol- d_4 , 175 MHz): δ 8.7 (CH_3); 67.5 (CH_2); 103.5 (C_2); 107.1 (C_6); 110.5 (C_4); 114.5 (C_6); 116.4 (C_2); 123.4 (C_4); 128.7 (C_5); 132.0 (C_5); 133.2 (C_4/C_5); 135.3 (C_4/C_5); 136.3 (C_3); 140.7 (C_3); 158.1 (C_3); 160.5, 160.6 (C_1 , C_1); 176.6 (C=O). HRMS (ESI, m/z): calcd for $\text{C}_{18}\text{H}_{14}\text{ClN}_2\text{O}_5$ [M-H] $^-$: 373.0597; found: 373.0577. HPLC (method B, t_R , min): 14.21.

[4-[4-(4-Chlorophenoxy)-5-methyl-1H-pyrazol-3-yl]-3-hydroxyphenoxy]acetic Acid (11). Following general procedures 5 and 6, pyrazole **11** was obtained from chromone **27** (14 mg, 0.04

mmol) in 99% yield. Chromatography: DCM to DCM/methanol, 8:2. Mp: 121–123 °C. R_f: 0.85 (DCM/methanol, 7:3). IR (ATR): ν 1627 (C=O). ¹H NMR (methanol-*d*₄, 700 MHz): δ 2.22 (s, 3H, CH₃); 4.69 (s, 2H, CH₂); 6.42 (dd, *J* = 8.9, 2.5, 1H, H₆); 6.51 (d, *J* = 2.5, 1H, H₂); 6.96 (d, *J* = 9.0, 2H, H_{2'}, H_{6'}); 7.30 (d, *J* = 9.0, 2H, H_{3'}, H_{5'}); 7.62 (d, *J* = 8.8, 1H, H₅). ¹³C NMR (methanol-*d*₄, 175 MHz): δ 8.5 (CH₃); 65.9 (CH₂); 103.3 (C₂); 107.3 (C₆); 108.3 (C₄); 117.7 (C_{2'}, C_{6'}); 128.9 (C_{4'}); 130.3 (C₅); 130.9 (C_{3'}, C_{5'}); 134.1, 137.3 (C_{4'}, C_{5'}); 138.3 (C₃); 157.6 (C_{1'}); 158.1 (C₃); 161.6 (C₁); 171.0 (C=O). HRMS (ESI, *m/z*): calcd for C₁₈H₁₄ClN₂O₅ [M-H]⁻: 373.0591; found: 373.0577. HPLC (method B, t_R, min): 23.78.

4-[4-(3,4-Dichlorophenoxy)-5-methyl-1H-pyrazol-3-yl]-3-hydroxyphenoxy}acetic Acid (12). Following general procedures 5 and 6, pyrazole 12 was obtained from chromone 28 (38 mg, 0.09 mmol) in 92% yield. Chromatography: ethyl acetate to ethyl acetate/methanol, 8:2. Mp: >240 °C (decomp.). R_f: 0.10 (ethyl acetate/methanol, 9:1). IR (ATR): ν 3406 (OH, NH); 1586 (C=O); 1258, 1174 (C–O–C). ¹H NMR (methanol-*d*₄, 700 MHz): δ 2.13 (s, 3H, CH₃); 4.41 (s, 2H, CH₂); 6.37 (dd, *J* = 8.7, 2.5, 1H, H₆); 6.47 (d, *J* = 2.5, 1H, H₂); 6.86 (dd, *J* = 9.0, 3.0, 1H, H_{6'}); 7.06 (d, *J* = 3.0, 1H, H_{2'}); 7.41 (d, *J* = 9.0, 1H, H_{5'}); 7.46 (d, *J* = 8.7, 1H, H₅). ¹³C NMR (methanol-*d*₄, 175 MHz): δ 8.6 (CH₃); 67.6 (CH₂); 103.5 (C₂); 107.2 (C₆); 110.3 (C₄); 116.2 (C_{6'}); 118.1 (C_{2'}); 126.4 (C_{4'}); 128.7 (C₅); 132.4 (C_{5'}); 133.1 (C_{4'/C_{5'}}); 134.1 (C_{4'/C_{5'}}, C_{3'}); 158.9 (C₃, C_{1'}); 160.8 (C₁); 176.9 (C=O); C₃ not observed. HRMS (ESI, *m/z*): calcd for C₁₈H₁₃Cl₂N₂O₅ [M-H]⁻: 407.0207; found: 407.0198. HPLC (method B, t_R, min): 15.86.

4-[4-(2,4-Dichlorophenoxy)-5-methyl-1H-pyrazol-3-yl]-3-hydroxyphenoxy}acetic Acid (13). Following general procedures 5 and 6, pyrazole 13 was obtained from chromone 29 (45 mg, 0.11 mmol) in 99% yield. Chromatography: DCM to DCM/methanol, 8:2. Mp: >196 °C (decomp.). R_f: 0.93 (DCM/methanol/acetic acid, 7:3:0.01). IR (ATR): ν 3413 (OH, NH); 1619 (C=O); 1182 (C–O–C). ¹H NMR (methanol-*d*₄, 300 MHz): δ 2.14 (s, 3H, CH₃); 4.60 (s, 2H, CH₂); 6.36 (dd, *J* = 8.7, 2.5, 1H, H₆); 6.47 (d, *J* = 2.5, 1H, H₂); 6.68 (d, *J* = 8.9, 1H, H_{6'}); 7.14 (dd, *J* = 8.9, 2.5, 1H, H_{5'}); 7.49–7.53 (m, 2H, H₃, H₅). ¹³C NMR (methanol-*d*₄, 125 MHz): δ 8.7 (CH₃); 66.5 (CH₂); 103.5 (C₂); 107.1 (C₆); 110.6 (C₄); 116.8 (C_{6'}); 124.1 (C_{2'}); 128.3 (C_{4'}); 128.6 (C₅); 129.1 (C_{5'}); 131.1 (C_{3'}); 133.2, 134.3 (C₄, C₅); 139.7 (C₃); 153.9 (C_{1'}); 158.1 (C₃); 160.4 (C₁); 173.8 (C=O). HRMS (ESI, *m/z*): calcd for C₁₈H₁₃Cl₂N₂O₅ [M-H]⁻: 407.0207; found: 407.0192. HPLC (method B, t_R, min): 14.90.

4-(2,4-Dichlorophenoxy)-3-(4-carboxymethoxyphenyl)-5-methyl-1H-pyrazole (30). A mixture of pyrazole 35 (10 mg, 0.02 mmol, 1 equiv.) and 1 M NaOH (30 μ L, 0.03 mmol, 1.5 equiv.) in 1,4-dioxane (1 mL) was stirred at 60° for 2 h. After cooling to rt, the mixture was treated with 1 M HCl until acidic pH and extracted with ethyl acetate (2×). The combined organic phases were washed with brine, dried over Na₂SO₄, filtered, and concentrated under reduced pressure. The crude was purified by flash chromatography (ethyl acetate/methanol, 8:2 to ethyl acetate/methanol, 7:3) to yield pure compound 30 in 99% yield. Mp: 158–160 °C. R_f: 0.13 (ethyl acetate/methanol, 7:3). IR (ATR): ν 3321 (NH/OH); 1649 (C=O); 1020 (C–O–C). ¹H NMR (methanol-*d*₄, 700 MHz): δ 2.11 (s, 3H, CH₃); 4.63 (s, 2H, CH₂); 6.66 (d, *J* = 8.9, 1H, H₆); 6.92 (d, *J* = 9.0, 2H, H₂, H₆); 7.12 (dd, *J* = 8.9, 2.5, 1H, H_{5'}); 7.50 (d, *J* = 2.5, 1H, H_{3'}); 7.62 (d, *J* = 9.0, 2H, H₃, H₅). ¹³C NMR (methanol-*d*₄, 175 MHz): δ 9.2 (CH₃); 66.1 (CH₂); 115.9 (C₂, C₆); 116.7 (C_{6'}); 124.1 (C_{2'}); 124.4 (C₄); 128.2 (C₃, C₅); 128.3 (C_{4'}); 129.1 (C_{5'}); 131.1 (C_{3'}); 133.7, 137.5 (C₄, C₅); 139.0 (C₃); 154.1 (C_{1'}); 159.5 (C₁); 173.0 (C=O). HRMS (ESI, *m/z*): calcd for C₁₈H₁₃Cl₂N₂O₄ [M-H]⁻: 391.0258; found: 391.0247. HPLC (method A, t_R, min): 17.53.

3-[4-[4-(2,4-Dichlorophenoxy)-5-methyl-1H-pyrazol-3-yl]-3-hydroxyphenoxy}propanoic Acid (36). Following general procedures 5 and 6, pyrazole 36 was obtained from chromone 39 (13 mg, 0.03 mmol) in 97% yield. Chromatography: ethyl acetate/methanol, 8:2. R_f: 0.83 (ethyl acetate/methanol, 8:2). IR (ATR): ν 2955, 2941 (NH, OH); 1653 (C=O); 1223 (C–O–C). ¹H NMR (methanol-*d*₄, 700 MHz): δ 2.20 (s, 3H, CH₃); 2.78 (t, *J* = 6.5, 2H, CH₂CO); 4.22 (t, *J*

= 6.5, 2H, OCH₂); 6.36 (dd, *J* = 8.8, 2.6, 1H, H₆); 6.53 (d, *J* = 2.6, 1H, H₂); 6.59 (d, *J* = 8.9, 1H, H_{6'}); 7.03 (dd, *J* = 8.9, 2.6, 1H, H_{5'}); 7.45 (d, *J* = 2.5, 1H, H_{3'}); 7.56 (d, *J* = 8.7, 1H, H₅). ¹³C NMR (methanol-*d*₄, 175 MHz): δ 8.6 (CH₃); 34.5 (CH₂CO); 63.4 (OCH₂); 102.6 (C₂); 106.8 (C₆); 109.0 (C₄); 115.7 (C_{6'}); 123.6 (C_{2'}); 127.6 (C_{4'}); 127.7 (C₅); 128.0 (C_{5'}); 130.5 (C_{3'}); 133.0, 135.0 (C₄, C₅); 140.0 (C₃); 152.4 (C_{1'}); 158.0 (C₃); 160.0 (C₁); 174.0 (C=O). HRMS (ESI, *m/z*): calcd for C₁₉H₁₅Cl₂N₂O₅ [M-H]⁻: 421.0364; found: 421.0370. HPLC (method B, t_R, min): 23.38.

4-[4-[4-(2,4-Dichlorophenoxy)-5-methyl-1H-pyrazol-3-yl]-3-hydroxyphenoxy}butanoic Acid (37). Following general procedures 5 and 6, pyrazole 37 was obtained from chromone 40 (12 mg, 0.03 mmol) in 99% yield. Chromatography: ethyl acetate to ethyl acetate/methanol, 8:2. R_f: 0.56 (ethyl acetate/methanol, 1:1). IR (ATR): ν 3431 (NH/OH); 1669 (C=O); 1263 (C–O–C). ¹H NMR (methanol-*d*₄, 700 MHz): δ 2.00–2.04 (m, 2H, CH₂); 2.13 (s, 3H, CH₃); 2.43 (t, *J* = 7.4, 2H, CH₂CO); 3.96 (t, *J* = 6.3, 2H, OCH₂); 6.35 (dd, *J* = 8.7, 2.6, 1H, H₆); 6.45 (d, *J* = 2.5, 1H, H₂); 6.69 (d, *J* = 8.9, 1H, H_{6'}); 7.14 (dd, *J* = 8.9, 2.5, 1H, H_{5'}); 7.48 (d, *J* = 8.8, 1H, H₅); 7.52 (d, *J* = 2.5, 1H, H_{3'}). ¹³C NMR (methanol-*d*₄, 175 MHz): δ 7.9 (CH₃); 26.1 (CH₂); 31.7 (CH₂CO); 68.1 (OCH₂); 103.2 (C₂); 107.1 (C₆); 109.1 (C₄); 116.8 (C_{6'}); 124.1 (C_{2'}); 128.3 (C₅, C_{4'}); 129.1 (C_{5'}); 131.1 (C_{3'}); 133.1, 134.2 (C₄, C₅); 154.0 (C_{1'}); 158.2 (C₃); 161.3 (C₁); 178.1 (C=O); C₃ not observed. MS (ESI, *m/z*): 435.0, 437.1, 439.0 [M-H]⁻. HPLC (method B, t_R, min): 23.33.

5-[4-[4-(2,4-Dichlorophenoxy)-5-methyl-1H-pyrazol-3-yl]-3-hydroxyphenoxy}pentanoic Acid (38). Following general procedures 5 and 6, pyrazole 38 was obtained from chromone 41 (140 mg, 0.30 mmol) in 86% yield. Chromatography: hexane/ethyl acetate 9:1 to hexane/ethyl acetate 1:1. R_f: 0.64 (ethyl acetate/methanol, 8:2). IR (ATR): ν 2923, 2852 (NH, OH); 1703 (C=O); 1242, 1191 (C–O–C). ¹H NMR (methanol-*d*₄, 700 MHz): δ 1.74–1.78 (m, 4H, 2CH₂); 2.13 (s, 3H, CH₃); 2.35 (t, *J* = 6.7, 2H, COCH₂); 3.94 (t, *J* = 5.5, 2H, OCH₂); 6.34 (dd, *J* = 8.7, 2.6, 1H, H₆); 6.44 (d, *J* = 2.5, 1H, H₂); 6.68 (d, *J* = 8.9, 1H, H_{6'}); 7.14 (dd, *J* = 8.9, 2.5, 1H, H_{5'}); 7.48 (d, *J* = 8.8, 1H, H₅); 7.52 (d, *J* = 2.5, 1H, H_{3'}). ¹³C NMR (methanol-*d*₄, 175 MHz): δ 8.3 (CH₃); 22.8, 29.8 (2CH₂); 34.7 (COCH₂); 68.5 (OCH₂); 103.2 (C₂); 107.1 (C₆); 109.8 (C₄); 116.8 (C_{6'}); 124.1 (C_{2'}); 128.3 (C₅); 128.6 (C_{4'}); 129.1 (C_{5'}); 131.1 (C_{3'}); 133.2 (C₅); 135.5 (C₄); 140.4 (C₃); 154.0 (C_{1'}); 156.0 (C₃); 161.4 (C₁); 177.5 (C=O). HRMS (ESI, *m/z*): calcd for C₂₁H₁₉Cl₂N₂O₅ [M-H]⁻: 449.0749; found: 449.0741. HPLC (method B, t_R, min): 18.34.

4-[4-(2,4-Dichlorophenoxy)-5-methyl-1H-pyrazol-3-yl]benzene-1,3-diol (42). Following general procedure 5, pyrazole 42 was obtained from chromone 25 (82 mg, 0.24 mmol) in 65% yield. Mp: 206–208 °C. R_f: 0.23 (ethyl acetate/methanol, 6:4). IR (ATR): ν 3293 (OH, NH); 1250 (C–O–C). ¹H NMR (CDCl₃, 700 MHz): δ 2.12 (s, 3H, CH₃); 6.21 (dd, *J* = 8.5, 2.1, 1H, H₆); 6.34 (d, *J* = 2.0, 1H, H₂); 6.66 (d, *J* = 8.9, 1H, H_{6'}); 7.11 (dd, *J* = 8.9, 2.4, 1H, H_{5'}); 7.40 (d, *J* = 8.6, 1H, H₅); 7.50 (d, *J* = 2.4, 1H, H_{3'}). ¹³C NMR (CDCl₃, 175 MHz): δ 8.7 (CH₃); 103.9 (C₂); 108.0 (C₆); 108.9 (C₄); 116.8 (C_{6'}); 124.1 (C_{2'}); 128.3 (C_{4'}); 128.6 (C₅); 129.1 (C_{5'}); 130.9 (C_{4'/C_{5'}}); 131.1 (C_{3'}); 133.0 (C_{4'/C_{5'}}); 153.9 (C₃); 158.1 (C_{1'}); 159.6 (C₁, C₃). HRMS (ESI, *m/z*): calcd for C₁₆H₁₃Cl₂N₂O₃ [M + H]⁺: 351.0298; found: 351.0303. HPLC (method B, t_R, min): 21.80.

2-[4-(2,4-Dichlorophenoxy)-5-methyl-1H-pyrazol-3-yl]-5-methoxyphenol (43). A mixture of pyrazole 42 (25 mg, 0.07 mmol, 1 equiv.), potassium carbonate (21 mg, 0.15 mmol, 2.1 equiv.) and iodomethane (10 μ L, 0.13 mmol, 1.8 equiv.) in acetone (0.84 mL) was stirred at 65 °C for 6 h. After cooling to rt, the solvent was evaporated under reduced pressure and the residue was dissolved in ethyl acetate and washed with water and brine. The organic phase was dried over Na₂SO₄, filtered, and concentrated under reduced pressure. The crude was purified by flash chromatography (hexane to hexane/ethyl acetate, 7:3) to yield pure compound 43 in 20% yield. Mp: 220–222 °C. R_f: 0.50 (ethyl acetate/methanol, 6:4). IR (ATR): ν 3352 (OH, NH); 1252 (C–O–C). ¹H NMR (methanol-*d*₄, 700 MHz): δ 2.15 (s, 3H, C₅CH₃); 3.85 (s, 3H, OCH₃); 6.18 (dd, *J* = 8.6, 2.5, 1H, H₄); 6.31 (d, *J* = 2.4, 1H, H₆); 6.68 (d, *J* = 8.9, 1H, H_{6'}); 7.14

(dd, $J = 8.9, 2.5, 1\text{H}, \text{H}_{5'}); 7.37$ (d, $J = 8.6, 1\text{H}, \text{H}_3$); 7.53 (d, $J = 2.5, 1\text{H}, \text{H}_3$). ^{13}C NMR (methanol- d_4 , 175 MHz): δ 8.1 ($\text{C}_5\text{-CH}_3$); 52.1 (OCH $_3$); 104.0 (C_6); 107.9 (C_4); 109.1 (C_2); 116.8 (C_6'); 124.1 (C_2'); 128.35 (C_3); 128.4 (C_4'); 129.1 (C_5'); 131.1 (C_3'); $132.8, 133.3$ (C_4, C_5); 141.6 (C_3); 153.9 (C_1'); $158.4, 159.5$ (C_1, C_5). HRMS (ESI, m/z): calcd for $\text{C}_{17}\text{H}_{15}\text{Cl}_2\text{N}_2\text{O}_3$ [$\text{M} + \text{H}$] $^+$: 365.0454; found: 365.0458. HPLC (method B, t_{R} , min): 21.90.

Methyl {4-[4-(2,4-dichlorophenoxy)-5-methyl-1H-pyrazol-3-yl]-3-hydroxyphenoxy} Acetate (44). To a solution of pyrazole **13** (293 mg, 0.94 mmol) in methanol (3.70 mL) was added conc. H_2SO_4 (31 μL), and the reaction was refluxed overnight. The mixture was diluted with ethyl acetate, washed with water and brine, dried over Na_2SO_4 , filtered, and concentrated under reduced pressure. The crude was purified by flash chromatography (hexane/ethyl acetate, 9:1 to hexane/ethyl acetate, 7:3) to yield pure compound **44** in 85% yield. Mp: >210 $^\circ\text{C}$ (decomp.). R_f : 0.98 (DCM/methanol/acetic acid, 8:2:0.1). IR (ATR): ν 3297 (OH, NH); 1634 (C=O); 1016 (C–O–C). ^1H NMR (methanol- d_4 , 500 MHz): δ 2.21 (s, 3H, $\text{C}_5\text{-CH}_3$); 3.77 (s, 3H, OCH $_3$); 4.69 (s, 2H, CH $_2$); 6.41 (dd, $J = 8.7, 2.6, 1\text{H}, \text{H}_6$); 6.49 (d, $J = 2.5, 1\text{H}, \text{H}_2$); 6.75 (d, $J = 8.9, 1\text{H}, \text{H}_6'$); 7.17 (dd, $J = 8.9, 2.5, 1\text{H}, \text{H}_5'$); 7.55 (d, $J = 8.8, 1\text{H}, \text{H}_3$); 7.57 (d, $J = 2.5, 1\text{H}, \text{H}_3'$). ^{13}C NMR (methanol- d_4 , 125 MHz): δ 8.5 ($\text{C}_5\text{-CH}_3$); 52.6 (OCH $_3$); 65.9 (CH $_2$); 103.4 (C_2); 107.2 (C_6); 108.8 (C_4); 116.9 (C_6'); 124.3 (C_2'); 129.0 (C_4'); 129.3 (C_5); 129.7 (C_5'); 131.3 (C_3'); $133.6, 137.5$ (C_4, C_5); 142.2 (C_3); 153.3 (C_1'); 158.2 (C_3); 161.3 (C_1); 171.0 (C=O). HRMS (ESI, m/z): calcd for $\text{C}_{19}\text{H}_{15}\text{Cl}_2\text{N}_2\text{O}_5$ [$\text{M}-\text{H}$] $^-$: 421.0363; found: 421.0343. HPLC (method B, t_{R} , min): 26.27.

2-[4-[4-(2,4-Dichlorophenoxy)-5-methyl-1H-pyrazol-3-yl]-3-hydroxyphenoxy]acetamide (45). Following the general procedure **5**, pyrazole **45** was obtained from chromone **46** (24 mg, 0.06 mmol) in 80% yield. R_f : 0.50 (ethyl acetate/methanol, 9:1). IR (ATR): ν 3413 (OH, NH); 1619 (C=O); 1182 (C–O–C). ^1H NMR (methanol- d_4 , 700 MHz): δ 2.14 (s, 3H, CH $_3$); 4.44 (s, 2H, CH $_2$); 6.42 (d, $J = 8.6, 1\text{H}, \text{H}_6$); 6.53 (d, $J = 2.5, 1\text{H}, \text{H}_2$); 6.68 (d, $J = 8.9, 1\text{H}, \text{H}_6'$); 7.14 (dd, $J = 8.9, 2.4, 1\text{H}, \text{H}_5'$); 7.52 (d, $J = 8.7, 1\text{H}, \text{H}_3$); 7.52 (d, $J = 2.4, 1\text{H}, \text{H}_3'$). ^{13}C NMR (methanol- d_4 , 175 MHz): δ 7.9 (CH $_3$); 67.8 (CH $_2$); 103.6 (C_2); 107.1 (C_6); 110.9 (C_4); 116.7 (C_6'); 124.1 (C_2'); 128.4 (C_4, C_5); 129.1 (C_5'); 131.1 (C_3'); $133.2, 136.3$ (C_5, C_4); 142.5 (C_3); 153.9 (C_1'); 158.3 (C_3); 159.8 (C_1); 173.9 (C=O). HRMS (ESI, m/z): calcd for $\text{C}_{18}\text{H}_{14}\text{Cl}_2\text{N}_3\text{O}_4$ [$\text{M}-\text{H}$] $^-$: 406.0440; found: 406.0356. HPLC (method B, t_{R} , min): 15.39.

4-[4-(2,4-Dichlorophenoxy)-1,5-dimethyl-1H-pyrazol-3-yl]-3-hydroxyphenoxy]acetic Acid (47). To a solution of pyrazole **13** (66 mg, 0.16 mmol, 1 equiv.) in anhydrous THF (0.70 mL) was added sodium hydride (60% dispersion in mineral oil, 8 mg, 0.32 mmol, 2 equiv.) at 0 $^\circ\text{C}$ and the mixture was stirred for 3 h, allowing it to reach rt during this time. Next, iodomethane (20 μL , 0.16 mmol, 1 equiv.) was added and the reaction was stirred at rt for 16 h. After this time, 1 M HCl was added until neutral pH and the organic solvent was evaporated. The residue was extracted with ethyl acetate (3 \times). The combined organic phases were washed with brine, dried over Na_2SO_4 , filtered, and concentrated under reduced pressure to obtain pure compound **47** in 31% yield. Chromatography: hexane/ethyl acetate, 4:6 to ethyl acetate. R_f : 0.16 (ethyl acetate/methanol/acetic acid, 9:1:0.01). IR (ATR): ν 2929 (OH); 1629 (C=O); 1261 (C–O–C). ^1H NMR (methanol- d_4 , 700 MHz): δ 2.16 (s, 3H, $\text{C}_5\text{-CH}_3$); 3.86 (s, 3H, NCH $_3$); 4.49 (s, 2H, CH $_2$); 6.34 (dd, $J = 8.8, 2.5, 1\text{H}, \text{H}_6$); 6.46 (d, $J = 2.5, 1\text{H}, \text{H}_2$); 6.67 (d, $J = 8.9, 1\text{H}, \text{H}_6'$); 7.13 (dd, $J = 8.9, 2.5, 1\text{H}, \text{H}_5'$); 7.46 (d, $J = 2.5, 1\text{H}, \text{H}_3$); 7.53 (d, $J = 8.7, 1\text{H}, \text{H}_3'$). ^{13}C NMR (methanol- d_4 , 175 MHz): δ 8.2 ($\text{C}_5\text{-CH}_3$); 37.2 (NCH $_3$); 67.2 (CH $_2$); 103.5 (C_2); 107.2 (C_6); 110.5 (C_4); 116.7 (C_6'); 124.0 (C_2'); 128.2 (C_4'); 128.5 (C_5'); 129.2 (C_5); 131.2 (C_3'); $133.0, 133.4$ (C_5, C_4); 141.2 (C_3); 153.8 (C_1'); 158.3 (C_3); 160.6 (C_1); 172.9 (C=O). HRMS (MALDI, m/z): calcd for $\text{C}_{19}\text{H}_{16}\text{Cl}_2\text{N}_2\text{O}_5$ [$\text{M} + \text{H}$] $^+$: 422.0436; found: 422.0433. HPLC (method B, t_{R} , min): 16.60.

4-[4-(2,4-Dichlorophenoxy)-1H-pyrazol-3-yl]-3-hydroxyphenoxy]acetic Acid (48). Following general procedures **5** and **6**, pyrazole **48** was obtained from chromone **51** (27 mg, 0.07 mmol) in 58% yield. Chromatography: ethyl acetate/methanol, 9:1 to ethyl acetate/methanol, 8:2. R_f : 0.10 (ethyl acetate/methanol, 7:3). IR

(ATR): ν 3187 (OH, NH); 1627 (C=O); 1226 (C–O–C). ^1H NMR (methanol- d_4 , 500 MHz): δ 4.42 (s, 2H, CH $_2$); 6.39 (dd, $J = 8.8, 2.5, 1\text{H}, \text{H}_6$); 6.49 (d, $J = 2.5, 1\text{H}, \text{H}_2$); 6.84 (d, $J = 8.9, 1\text{H}, \text{H}_6'$); 7.16 (dd, $J = 8.9, 2.5, 1\text{H}, \text{H}_5'$); 7.50 (d, $J = 2.5, 1\text{H}, \text{H}_3$); 7.57 (d, $J = 8.7, 1\text{H}, \text{H}_3$); 7.61 (s, 1H, H_5'). ^{13}C NMR (methanol- d_4 , 125 MHz): δ 67.8 (CH $_2$); 103.5 (C_2); 107.2 (C_6); 110.1 (C_4); 117.8 (C_6'); 124.7 (C_2'); 128.7 (C_4'); 128.9 (C_5, C_5'); 129.1 (C_5'); 131.1 (C_3'); 136.6 (C_4); 154.4 (C_1'); 157.9 (C_3); 160.8 (C_1); 176.5 (C=O); C_3 , not observed. HRMS (ESI, m/z): calcd for $\text{C}_{17}\text{H}_{11}\text{Cl}_2\text{N}_2\text{O}_5$ [$\text{M}-\text{H}$] $^-$: 393.0050; found: 393.0017. HPLC (method B, t_{R} , min): 21.11.

4-[4-(2,4-Dichlorophenoxy)-3-methyl-1,2-oxazol-3-yl]-3-hydroxyphenoxy]acetic Acid (49). To a solution of isoxazole **52** (7 mg, 0.02 mmol, 1 equiv.) in the minimum amount of 1,4-dioxane was added 1 M NaOH (0.20 mL, 0.20 mmol, 10 equiv.), and the reaction was heated at 60 $^\circ\text{C}$ overnight. After cooling to rt, the solvent was removed under reduced pressure. The residue was dissolved with ethyl acetate and washed with a 1 M HCl solution and brine, dried over Na_2SO_4 , filtered, and concentrated under reduced pressure, affording the corresponding isoxazole **49** in 91% yield. Mp: >210 $^\circ\text{C}$ (decomp.). R_f : 0.15 (ethyl acetate/methanol/acetic acid, 7:3:0.01). IR (ATR): ν 2919 (OH); 1729 (C=O); 1175 (C–O–C). ^1H NMR (methanol- d_4 , 500 MHz): δ 2.13 (s, 3H, CH $_3$); 4.63 (s, 2H, OCH $_2$); 6.41 (d, $J = 2.4, 1\text{H}, \text{H}_2$); 6.51 (dd, $J = 8.7, 2.5, 1\text{H}, \text{H}_6$); 6.87 (d, $J = 8.9, 1\text{H}, \text{H}_6'$); 7.17 (dd, $J = 8.9, 2.5, 1\text{H}, \text{H}_5'$); 7.38 (d, $J = 8.7, 1\text{H}, \text{H}_3$); 7.47 (dd, $J = 2.5, 1\text{H}, \text{H}_3'$). ^{13}C NMR (methanol- d_4 , 125 MHz): δ 9.2 (CH $_3$); 65.9 (OCH $_2$); 103.2 (C_2); 107.3 (C_6); 108.5 (C_4); 117.6 (C_6'); 124.4 (C_2'); 128.7 (C_4'); 128.8 (C_5'); 131.0 (C_5); 131.1 (C_3'); 132.2 (C_4); 153.4 (C_1'); 156.7 (C_5); $158.1, 158.9$ (C_3, C_3'); 162.5 (C_1); 172.4 (C=O). HRMS (MALDI, m/z): calcd for $\text{C}_{18}\text{H}_{13}\text{Cl}_2\text{NO}_6$ [$\text{M} + \text{H}$] $^+$: 409.0120; found: 409.0127. HPLC (method B, t_{R} , min): 11.48.

4-[4-(2,4-Difluorophenoxy)-5-methyl-1H-pyrazol-3-yl]-3-hydroxyphenoxy]acetic Acid (53). Following general procedures **5** and **6**, compound **53** was obtained from chromone **59** (65 mg, 0.17 mmol) in 61% yield. Chromatography: ethyl acetate to ethyl acetate/methanol 8:2. Mp: >210 $^\circ\text{C}$ (decomp.). R_f : 0.15 (ethyl acetate/methanol 8:2). IR (ATR): ν 3400 (OH); 1620 (C=O); 1246, 1190 (C–O–C). ^1H NMR (methanol- d_4 , 700 MHz): δ 2.14 (s, 3H, CH $_3$); 4.43 (s, 2H, CH $_2$); 6.37 (dd, $J = 9.0, 2.5, 1\text{H}, \text{H}_6$); 6.47 (d, $J = 2.5, 1\text{H}, \text{H}_2$); 6.71 (td, $J = 9.2, 5.3, 1\text{H}, \text{H}_6'$); 6.74 – 6.77 (m, 1H, H_5'); 7.09 (ddd, $J = 11.5, 9.0, 3.0, 1\text{H}, \text{H}_3$); 7.53 (d, $J = 8.5, 1\text{H}, \text{H}_3$). ^{13}C NMR (methanol- d_4 , 175 MHz): δ 8.6 (CH $_3$); 67.5 (CH $_2$); 103.4 (C_2); 106.0 (dd, $J = 27.5, 22.0, \text{C}_3'$); 107.1 (C_6); 110.5 (C_4); 111.8 (dd, $J = 23.0, 3.5, \text{C}_5'$); 117.2 (d, $J = 9.5, \text{C}_6'$); 128.6 (C_3); $133.5, 1135.7$ (C_4, C_5); 140.5 (C_3); 143.9 (dd, $J = 10.5, 3.0, \text{C}_1'$); 153.0 (dd, $J = 248.5, 12.0, \text{C}_2'$); 158.1 (C_3); 158.5 (dd, $J = 241.5, 10.0, \text{C}_4'$); 160.7 (C_1); 176.3 (C=O). HRMS (ESI, m/z): calcd for $\text{C}_{18}\text{H}_{13}\text{F}_2\text{N}_2\text{O}_5$ [$\text{M}-\text{H}$] $^-$: 375.0798; found: 375.0792. HPLC (method B, t_{R} , min): 13.33.

2-[4-(2,4-Dichlorophenoxy)-5-methyl-1H-pyrazol-3-yl]-5-[1H-tetrazol-5-yl]methoxy] Phenol (54). Following general procedure **7**, compound **54** was obtained from pyrazole **62** (262 mg, 0.70 mmol) in 72% yield. Chromatography: ethyl acetate/methanol, 9:1 to ethyl acetate/methanol, 6:4. Mp: 180–182 $^\circ\text{C}$. R_f : 0.19 (ethyl acetate/methanol, 8:2). IR (ATR): ν 2921 (NH, OH); 1238 (C–O–C). ^1H NMR (methanol- d_4 , 300 MHz): δ 2.14 (s, 3H, CH $_3$); 5.40 (s, 2H, CH $_2$); 6.49 (dd, $J = 8.7, 2.6, 1\text{H}, \text{H}_4$); 6.59 (d, $J = 2.6, 1\text{H}, \text{H}_6$); 6.68 (d, $J = 8.9, 1\text{H}, \text{H}_6'$); 7.14 (dd, $J = 8.9, 2.5, 1\text{H}, \text{H}_5'$); 7.52 – 7.56 (m, 2H, H_3, H_3'). ^{13}C NMR (methanol- d_4 , 75 MHz): δ 8.5 (CH $_3$); 60.8 (CH $_2$); 103.7 (C_6); 107.0 (C_4); 111.4 (C_2); 116.8 (C_6'); 124.1 (C_2'); 128.4 (C_4'); 128.8 (C_5'); 129.1 (C_3); 131.1 (C_3'); $133.3, 134.9$ (C_4, C_5); 140.2 (C_3); 153.9 (C_1'); 156.9 ($\text{C}_{\text{tetrazole}}$); 158.3 (C_1); 159.8 (C_5). HRMS (MALDI, m/z): calcd for $\text{C}_{18}\text{H}_{15}\text{Cl}_2\text{N}_6\text{O}_3$ [$\text{M} + \text{H}$] $^+$: 433.0504; found: 433.0506. HPLC (method C, t_{R} , min): 10.38.

2-[4-(2,4-Difluorophenoxy)-5-methyl-1H-pyrazol-3-yl]-5-[1H-tetrazol-5-yl]methoxy] Phenol (55). Following general procedure **7**, compound **55** was obtained from pyrazole **63** (344 mg, 0.96 mmol) in 52% yield. Chromatography: ethyl acetate/methanol, 9:1 to ethyl acetate/methanol, 6:4. Mp: >210 $^\circ\text{C}$ (decomp.). R_f : 0.47 (hexane/ethyl acetate, 4:6). IR (ATR): ν 2931 (OH, NH); 1252, 1190 (C–

O–C). ^1H NMR (methanol- d_4 , 300 MHz): δ 2.15 (s, 3H, CH_3); 5.40 (s, 2H, OCH_2); 6.51 (dd, $J = 8.7, 2.6$, 1H, H_4); 6.59 (d, $J = 2.6$, 1H, H_6); 6.72–6.77 (m, 2H, H_5 , H_6); 7.10 (td, $J = 9.5, 8.3, 2.5$, 1H, H_7); 7.60 (d, $J = 8.6$, 1H, H_3). ^{13}C NMR (methanol- d_4 , 75 MHz): δ 8.5 (CH_3); 60.8 (OCH_2); 103.7 (C_6); 106.0 (dd, $J = 27.5, 22.0$, C_3); 107.0 (C_4); 110.4 (C_2); 111.7 (dd, $J = 26.4, 3.3$, C_5); 117.2 (dd, $J = 9.5, 1.9$, C_6); 128.8 (C_3); 133.7, 134.6 (C_4 , C_5); 141.2 (C_3); 143.8 (dd, $J = 11.1, 3.2$, C_1); 153.1 (dd, $J = 248.7, 12.2$, C_2); 155.3 ($\text{C}_{\text{tetrazole}}$); 158.3 (C_1); 158.6 (dd, $J = 241.8, 10.2$, C_4); 159.7 (C_5). ^{19}F -NMR (methanol- d_4 , 282 MHz): δ -132.5, -120.5. HRMS (ESI, m/z): calcd for $\text{C}_{18}\text{H}_{15}\text{F}_2\text{N}_6\text{O}_3$ [$\text{M} + \text{H}$] $^+$: 401.1095; found: 401.1105. HPLC (method C, t_{R} , min): 9.20.

Evaluation of Receptor Activation by Ca^{2+} Mobilization Assay. Cells stably expressing the corresponding LPA_{1-3} receptor were grown as described previously.¹⁸ Changes in intracellular calcium levels were measured by using the fluorescent calcium sensitive dye Fluo-4 NW (Invitrogen). RH7777 cells or B103 cells were plated on poly-D-lysine or collagen coated, respectively, black-wall clear-bottom 96-well plates (Corning) at a density of 50 000 cells/well and cultured overnight. The culture medium was then replaced with 100 μL of Fluo-4 NW dye loading solution containing 2.5 μM of probenecid and incubated for 30 min at 37 $^\circ\text{C}$ followed by an additional 30 min at rt. Then, 20 μL of the test compound from a 6 \times stock solution in assay buffer were added and fluorescence was measured during 120 s after which 10 μM of LPA (18:1, 1-oleoyl-*sn*-glycerol-3-phosphate) was added and wells were monitored for additional 120 s. Fluorescence changes were registered in a FluoStar Optima instrument (BMG Labtech) at 525 nm using an excitation wavelength of 494 nm. Ca^{2+} transient increase was quantified by calculating the difference between maximum (stimulation with LPA 10 μM) and baseline values for each well, and antagonist activity was quantified by determining the percentage of the signal suppression caused by the compound under study with respect to the Ca^{2+} increase induced by LPA (which was considered 100%). As positive controls, 10 μM LPA and 10 μM ionomycin were included in every experiment. At this concentration, LPA induced a response about 30–33% of the one shown by ionomycin, which is in agreement with previously described results.²⁹ The data presented are from two to four independent experiments carried out in triplicate or quadruplicate. Dose–response curves were generated and IC_{50} values calculated by nonlinear regression analysis using *Prism* software version 5 (GraphPad Software Inc., San Diego, CA, USA).

The agonist activity at LPA_2 receptors was determined at 10 μM concentration for all final compounds as previously described.¹⁸

Binding Affinity at LPA_{4-6} . A free solution assay,^{23,24} where the lysophosphatidic acid receptor ($\text{LPA}_{2,4-6}$) containing nanovesicles (of 110–130 nm size as measured by dynamic light scattering) and compound under study are freely moving into solution was prepared to determine the equilibrium binding constants (K_{D}) in a native environment of the binding partners (ligand/compound–receptor). The assay was analyzed using a benchtop Compensated Interferometric Reader (CIR) that measured the light refractive index (ΔRI) change from binding-induced conformational and/or hydration changes produced by real time binding events in a sample (receptor containing nanovesicles plus compound) and compared to a nonbinding reference (RI matched buffer plus compound).³⁰ Finally, the interferometric signal from vector nanovesicles binding (non-specific) to compound was subtracted from the $\text{LPA}_{2,4-6}$ containing nanovesicles binding (total) to compound, to determine the specific binding interactions of the compounds to $\text{LPA}_{2,4-6}$. The concentration-dependent change in RI (ΔRI) signal from the compounds to $\text{LPA}_{2,4-6}$ or vector was fitted using the single site total vs nonspecific binding isotherm using GraphPad *Prism*. Specific K_{D} values were determined by fitting the total minus nonspecific signal to a single site binding isotherm.

The detailed free solution assay method was described previously.^{25,26} All the compounds were dissolved in 100% DMSO, aliquoted, and frozen at -80 $^\circ\text{C}$ for 1 week. The compound dilution series was freshly prepared in 0.5% DMSO/PBS (pH 7.4) to keep the maximum compound in solution. In the final assay, total protein

concentration was maintained at 25 $\mu\text{g}/\text{mL}$ with 0, 0.08, 0.4, 2, 10, 50, and 250 nM concentrations of the compound in a final buffer composition of 0.25% DMSO/PBS. Receptor-compound mixture was incubated at rt for about an hour on a shaker and then filled in a dropix sample well tray in the format of reference then sample and finally introduced to CIR using an automated Mitos Dropix (Dolomite Microfluidics, UK) sample introducer. The detailed description of the CIR was mentioned elsewhere.^{31,32} It is a benchtop RI reader that combined a compensated interferometer with a Mitos Dropix (an automated droplet generator) and a syringe pump. The compensated interferometer, which consisted of a diode laser, one or two mirrors, one glass capillary, and a CCD camera, measures the RI change from a solution undergoing conformational and/or hydration alteration compared to a reference (with no such binding events). ΔRI is measured by capturing the translational shifts in backscattered light interference fringes produced from the interaction between an expanded beam profile of the laser and a capillary filled with droplets of sample-reference solutions. The positional shift of the back-scattered fringes, which is equivalent to molecular interaction, was quantified using fast Fourier transform of selected bright fringes captured in a CCD camera. The data acquisition and analysis were performed using a LabVIEW interface designed at the laboratory.

In Silico Experiments. Docking calculations were performed using *Autodock4*³³ [using: ga_num_evals (depending on the number of rotatable bonds) = 6 310 000 (for compounds 3, 13, 53, 54, 55) and 25 000 000 (for compound 38), $\text{ga_run} = 100$ and all the other parameters set to their default values]. The LPA_2 receptor model was generated using SwissModel³⁴ and the crystal structure with PDB ID 4Z35¹⁹ as a template. The generated model was prepared for docking using *pdb 2pqr*^{35,36} with the *propka*^{37,38} protonation option at a pH of 7.4 and the *poepb* force field.³⁹ All the analyzed compounds were modeled using *RDKit* (Open-source cheminformatics) and its protonation state adjusted at pH 7.4 by the ChemAxon *cxcalc* module (command line version of ChemAxon's *Calculator Plugins*, v16.10.24.0, 2016). Binding mode pictures were created using *PyMOL* v2.5.0.

Mutagenesis Experiments. Amino terminal hemagglutinin (HA)-tagged LPA_2 point mutants K22A, R107A, Q108A, and K278A containing pcDNA3.1 plasmids were provided by GenScript. For expression of the different constructs, McA-RH7777 (CRL-1601, ATCC) cells were selected, as they have been previously used for point mutation experiments of LPA receptors.⁴⁰ Cells were grown in Dulbecco's modified Eagle's medium supplemented with 10% (v/v) fetal bovine serum and 1% (v/v) penicillin-streptomycin and kept at 37 $^\circ\text{C}$ and 5% CO_2 . Cells were transiently transfected with the different plasmids using lipofectamine and following the manufacturer's procedure. Successful transfection was confirmed by flow cytometry analysis. For these experiments, 1×10^5 cells were resuspended in 50 μL of PBS with 2 mM EDTA and 0.5% BSA. Anti-HA antibody (Santa Cruz, sc-7392; 1 μg per 1×10^6 cells) was added and cells were incubated for 30 min at rt with shaking. Cells were centrifuged, washed with buffer, and incubated with antimouse Alexa Fluor 488 (Invitrogen, 1:5000) for 30 min at rt with shaking and protected from light. Cells were centrifuged, washed with buffer, resuspended in 0.3 mL of buffer and analyzed by flow cytometry in a FACScalibur instrument (Becton Dickinson) at the UCM's microscopy and flow cytometry unit. After confirming the transfection by flow cytometry, calcium mobilization experiments were carried out as previously described.

Permeability and Microsomal Stability. These studies were carried out as previously described with minor modifications.^{41,42} The assessment of the membrane permeability of synthesized compounds and propranolol and metoprolol as reference compounds was performed in a commercially available 96-well Corning Gentest precoated PAMPA plate system (Cultek S.L.U., Spain). Prior to use, the precoated PAMPA plate system was warmed to rt for 30 min and 300 μL of 200 μM solution of tested compound in 2% DMSO in PBS (pH 7.4) were added into wells in the receiver (donor) plate. Then, 200 μL of PBS were added into wells in the filter (acceptor) plate. The filter plate was placed on the receiver plate by slowly lowering the

precoated PAMPA plate until it sits on the receiver plate. The assembly was incubated at rt for 5 h, and then buffer samples were collected carefully from each plate. The final concentrations of compound in both donor and acceptor wells were analyzed by HPLC-MS and quantification was estimated by using the peak area integration normalized with an internal standard. Permeability value of the compounds was calculated using the following formula: P (cm/s) = $\{-\ln[1 - C_A(t)/C_{eq}]\}/[A(1/V_D + 1/V_A)t]$, where A = filter area (0.3 cm²), V_D = donor well volume (0.3 mL), V_A = acceptor well volume (0.2 mL), t = incubation time (s), $C_A(t)$ = compound concentration (μ M) in the acceptor well at time t , $C_D(t)$ = compound concentration (μ M) in donor well at time t , and $C_{eq} = [C_D(t)V_D + C_A(t)V_A]/(V_D + V_A)$. Assays were performed in duplicate, and the compound was tested in two different plates on different days.

For measuring the stability in mouse and human liver microsomes, compounds were incubated at 37 °C at a final concentration of 1 or 5 μ M in PBS, respectively, together with a solution of nicotinamide adenine dinucleotide phosphate (NADPH) in PBS (final concentration of 2 mM) and a solution of MgCl₂ in PBS (final concentration of 5 mM). Reactions were initiated by the addition of a suspension of mouse liver microsomes (MLMs) (male CD-1 mice pooled, Sigma-Aldrich) or human liver microsomes (HLMs) (male human pooled, Sigma-Aldrich), respectively, at a final protein concentration of 1 mg/mL. The solutions were vortexed and incubated at 37 °C. Aliquots of 100 μ L were quenched at time zero and at seven points ranging to 2 h (MLM) or 4 h (HLM) by pouring into 100 μ L of ice-cold acetonitrile. Quenched samples were centrifuged at 10 000g for 10 min, and the supernatants were filtered through a polytetrafluoroethylene (PTFE) membrane syringe filter (pore size of 0.2 μ m, 13 mm in diameter, GE Healthcare Life Sciences). The relative disappearance of the compound under study over the course of the incubation was monitored by HPLC-MS using SIM mode. Concentrations were quantified by measuring the area under the peak ($[M + H]^+$) normalized with an internal standard and converted to the percentage of compound remaining, using the time zero peak area value as 100%. The natural logarithm of the remaining percentage versus time data for each compound was fit to a linear regression, and the slope was used to calculate the degradation half-life ($t_{1/2}$).

Determination of the In Vivo Levels of Compound.

Compound **54** was administered intraperitoneally (25 mg/kg) in adult female 12–16 weeks old C57Bl/6j mice. At 1, 2, and 4 h after drug administration ($n = 3$ for each time and sample), mice were sacrificed and their brains, spinal cords, and blood were obtained. The brain and spinal cord were immediately frozen and kept at –80 °C until analysis. Blood was allowed to clot at rt for 30 min and centrifuged at 4 °C for 10 min at 16 000g. Serum was transferred to a clean polypropylene tube and stored at –80 °C until analysis. For analysis, a volume of cold acetonitrile was added to the serum. The sample was incubated in an ice bath for 10 min and centrifuged at 4 °C for 10 min at 16 000g. The resulting organic layer was filtered through a PTFE filter (0.2 μ m, 13 mm diameter, Fisher Scientific) and 20 μ L of the sample analyzed by LC-MS/MS at the UCM's Mass Spectrometry CAI. Separation was performed using a Phenomenex Gemini 5 μ m C18 110A 150 \times 2 mm column (run time 8 min; flow 0.5 mL/min; gradient: 0.5 min 10% Phase B, 2 min 60% Phase B, 4.5–6 min 100% Phase B, 7–8 min 10% Phase B; Phase A: water with formic acid 0.1%; Phase B: acetonitrile). The entire LC eluent was directly introduced to an electrospray ionization (ESI) source operating in the positive ion mode for LC MS/MS analysis on a Shimadzu LCMS8030 triple quadrupole mass spectrometer coupled to UHPLC with an oven temperature of 31.5 °C. The mass spectrometer ion optics were set in the multiple reaction monitoring mode and the transition selected for quantification was 432.90 > 215.10 (CE: –30 V).

Spinal Cord Injury In Vivo Model. All Surgical Procedures Were Approved by the Universitat Autònoma De Barcelona Animal Care Committee (CEEAH 4273) and followed the guidelines of the European Commission on Animal Care (EU Directive 2010/63/EU). Adult female C57Bl/6j mice (10–12 weeks old) and LPA₂ null mice

were anesthetized by intramuscular injection with a mixture of ketamine and xylazine (90:10 mg/kg). A laminectomy was performed at the 11th thoracic vertebrae and the exposed spinal cord was contused using the Infinite Horizon Impactor device (Precision Scientific Instrumentation) using a force of 60 kdynes. Only mice showing a spinal cord tissue displacement ranging between 450 and 550 μ m were selected. One hour after injury, compound **54** was injected intraperitoneally (25 mg/kg) which was then repeated daily for 10 consecutive days.

■ ASSOCIATED CONTENT

Supporting Information

The Supporting Information is available free of charge at <https://pubs.acs.org/doi/10.1021/acs.jmedchem.2c00046>.

Representative agonist curves for compounds **1**, **13**, and **54** (Figure S1); dose–activity curves for compounds **13**, **44**, and **53–55** (Figure S2); representative plots of FSA-CIR signal vs ligand concentration for the determination of affinity constants of compound **54** (Figure S3); numbered structures used in the structural characterization by NMR of all final compounds (Figure S4); HPLC gradients employed in HPLC-MS analysis of all tested compounds (Table S1); detailed synthetic procedures and characterization data of all intermediates; NMR spectra and HPLC trace analysis of final compounds (PDF)

PDB files of the structure of the LPA₂ receptor and select compounds from this study (ZIP)

Molecular formula strings (CSV)

■ AUTHOR INFORMATION

Corresponding Authors

Silvia Ortega-Gutiérrez – Departamento de Química Orgánica I, Facultad de Ciencias Químicas, Universidad Complutense de Madrid, Madrid E-28040, Spain; orcid.org/0000-0002-0257-6754; Email: siortega@ucm.es

María L. López-Rodríguez – Departamento de Química Orgánica I, Facultad de Ciencias Químicas, Universidad Complutense de Madrid, Madrid E-28040, Spain; orcid.org/0000-0001-8607-1085; Email: mluzlr@ucm.es

Authors

Nora Khiar-Fernández – Departamento de Química Orgánica I, Facultad de Ciencias Químicas, Universidad Complutense de Madrid, Madrid E-28040, Spain

Debora Zian – Departamento de Química Orgánica I, Facultad de Ciencias Químicas, Universidad Complutense de Madrid, Madrid E-28040, Spain

Henar Vázquez-Villa – Departamento de Química Orgánica I, Facultad de Ciencias Químicas, Universidad Complutense de Madrid, Madrid E-28040, Spain; orcid.org/0000-0001-7911-3160

R. Fernando Martínez – Departamento de Química Orgánica I, Facultad de Ciencias Químicas, Universidad Complutense de Madrid, Madrid E-28040, Spain; orcid.org/0000-0002-3278-6074

Andrea Escobar-Peña – Departamento de Química Orgánica I, Facultad de Ciencias Químicas, Universidad Complutense de Madrid, Madrid E-28040, Spain

Román Foronda-Sainz – Departamento de Química Orgánica I, Facultad de Ciencias Químicas, Universidad Complutense de Madrid, Madrid E-28040, Spain

Manisha Ray – Translational Neuroscience Initiative, Sanford Burnham Prebys Medical Discovery Institute, La Jolla, California 92037, United States

Maria Puigdomenech-Poch – Departament de Biologia Cel·lular, Fisiologia i Immunologia, Institut de Neurociències, Centro de Investigación Biomédica en Red sobre Enfermedades Neurodegenerativas (CIBERNED), Universitat Autònoma de Barcelona, Barcelona E-08193, Spain

Giovanni Cincilla – Molomics, Barcelona E-08028, Spain; orcid.org/0000-0002-5242-0707

Melchor Sánchez-Martínez – Molomics, Barcelona E-08028, Spain; Burua Scientific, Sant Pere de Ribes E-08810, Spain; orcid.org/0000-0002-3674-8577

Yasuyuki Kihara – Translational Neuroscience Initiative, Sanford Burnham Prebys Medical Discovery Institute, La Jolla, California 92037, United States

Jerold Chun – Translational Neuroscience Initiative, Sanford Burnham Prebys Medical Discovery Institute, La Jolla, California 92037, United States

Rubèn López-Vales – Departament de Biologia Cel·lular, Fisiologia i Immunologia, Institut de Neurociències, Centro de Investigación Biomédica en Red sobre Enfermedades Neurodegenerativas (CIBERNED), Universitat Autònoma de Barcelona, Barcelona E-08193, Spain; orcid.org/0000-0001-7615-9550

Complete contact information is available at:

<https://pubs.acs.org/10.1021/acs.jmedchem.2c00046>

Author Contributions

[†]N.K.-F. and D.Z. contributed equally. The manuscript was written through the contributions of all authors. M.L.L.-R., S.O.-G., and H.V.-V. designed the study and analyzed data. N.K.-F. and D.Z. contributed new reagents and analytic tools, determined LPA_{1–3} receptor activity, carried out pharmacokinetic assays, and analyzed data. R.F.M. and A.E.-P. contributed new reagents and analytic tools. R.F.-S. and S.O.-G. carried out the mutagenesis studies. G.C. and M.S.-M. performed molecular modeling studies and analyzed data. M.R., Y.K., and J.C. determined the LPA_{2,4–6} affinity and analyzed data. M.P.-P. and R.L.-V. performed the in vivo experiments and analyzed data. All authors have given approval to the final version of the manuscript.

Notes

The authors declare no competing financial interest.

ACKNOWLEDGMENTS

This work has been supported by the Spanish Ministerio de Ciencia, Innovación y Universidades (PID2019-106279RB-I00 to M.L.L.-R. and S.O.-G., PID2020-120267RB-I00 to R.L.-V., predoctoral FPU grants to N.K.-F., D.Z., and A.E.-P., and Juan de la Cierva postdoctoral fellowship to R.F.M.), Comunidad de Madrid (PEJ Program) to R.F.-S., and grants from the National Institute of Health (NIH) R01NS103940 (Y.K.) and R01NS084398, R01MH051699 and Department of Defense DOD W81XWH-17-1-0455 (J.C.). R.L.-V. is the recipient of an ICREA Academia award.

DEDICATION

This paper is dedicated to Prof. Joan Bosch on the occasion of his 75th birthday.

ABBREVIATIONS USED

BMS, Basso Mouse Scale; CNS, central nervous system; E_{max} , maximal receptor activation; FSA-CIR, free solution assay-compensated interferometric reader; GPCR, G protein-coupled receptor; HLM, human liver microsome; IC₅₀, concentration of compound that inhibit the 50% of the activation induced by LPA; i.p., intraperitoneally; LPA, lysophosphatidic acid; MLM, mouse liver microsome; MW, microwave; N.E., no effect; P, permeability; PK, pharmacokinetic; SCI, spinal cord injury; s.e.m., standard error of the mean

REFERENCES

- (1) Ahuja, C. S.; Wilson, J. R.; Nori, S.; Kotter, M. R. N.; Druschel, C.; Curt, A.; Fehlings, M. G. Traumatic spinal cord injury. *Nat. Rev. Dis. Primers* **2017**, *3*, 17018.
- (2) Hutson, T. H.; Di Giovanni, S. The translational landscape in spinal cord injury: focus on neuroplasticity and regeneration. *Nat. Rev. Neurol.* **2019**, *15*, 732–745.
- (3) Fehlings, M. G.; Chen, Y.; Aarabi, B.; Ahmad, F.; Anderson, K. D.; Dumont, T.; Fournay, D. R.; Harrop, J. S.; Kim, K. D.; Kwon, B. K.; Lingam, H. K.; Rizzo, M.; Shih, L. C.; Tsai, E. C.; Vaccaro, A.; McKerracher, L. A randomized controlled trial of local delivery of a Rho inhibitor (VX-210) in patients with acute traumatic cervical spinal cord injury. *J. Neurotrauma* **2021**, *38*, 2065–2072.
- (4) Liu, Z.; Yang, Y.; He, L.; Pang, M.; Luo, C.; Liu, B.; Rong, L. High-dose methylprednisolone for acute traumatic spinal cord injury: A meta-analysis. *Neurology* **2019**, *93*, e841–e850.
- (5) López-Vales, R.; David, S. Bioactive lipids in inflammation after central nervous system injury. *Adv. Exp. Med. Biol.* **2019**, *1127*, 181–194.
- (6) David, S.; López-Vales, R. Bioactive lipid mediators in the initiation and resolution of inflammation after spinal cord injury. *Neuroscience* **2021**, *466*, 273–297.
- (7) Yung, Y. C.; Stoddard, N. C.; Mirendil, H.; Chun, J. Lysophosphatidic acid signaling in the nervous system. *Neuron* **2015**, *85*, 669–682.
- (8) Santos-Nogueira, E.; López-Serrano, C.; Hernández, J.; Lago, N.; Astudillo, A. M.; Balsinde, J.; Estivill-Torrús, G.; de Fonseca, F. R.; Chun, J.; López-Vales, R. Activation of lysophosphatidic acid receptor type 1 contributes to pathophysiology of spinal cord injury. *J. Neurosci.* **2015**, *35*, 10224–10235.
- (9) Choi, J. W.; Herr, D. R.; Noguchi, K.; Yung, Y. C.; Lee, C. W.; Mutoh, T.; Lin, M. E.; Teo, S. T.; Park, K. E.; Mosley, A. N.; Chun, J. LPA receptors: subtypes and biological actions. *Annu. Rev. Pharmacol. Toxicol.* **2010**, *50*, 157–186.
- (10) Kihara, Y.; Maceyka, M.; Spiegel, S.; Chun, J. Lysophospholipid receptor nomenclature review: IUPHAR Review 8. *Br. J. Pharmacol.* **2014**, *171*, 3575–3594.
- (11) González-Gil, I.; Zian, D.; Vázquez-Villa, H.; Ortega-Gutiérrez, S.; López-Rodríguez, M. L. The status of the lysophosphatidic acid receptor type 1 (LPA1R). *MedChemComm.* **2015**, *6*, 13–26.
- (12) Suardiá, M.; Galan-Arriero, I.; Avila-Martin, G.; Estivill-Torrús, G.; de Fonseca, F. R.; Chun, J.; Gómez-Soriano, J.; Bravo-Esteban, E.; Taylor, J. Spinal cord compression injury in lysophosphatidic acid 1 receptor-null mice promotes maladaptive pronociceptive descending control. *Eur. J. Pain* **2016**, *20*, 176–185.
- (13) López-Serrano, C.; Santos-Nogueira, E.; Francos-Quijorna, I.; Coll-Miró, M.; Chun, J.; López-Vales, R. Lysophosphatidic acid receptor type 2 activation contributes to secondary damage after spinal cord injury in mice. *Brain Behav. Immun.* **2019**, *76*, 258–267.
- (14) Beck, H. P.; Kohn, T.; Rubenstein, S.; Hedberg, C.; Schwandner, R.; Hasslinger, K.; Dai, K.; Li, C.; Liang, L.; Wesche, H.; Frank, B.; An, S.; Wickramasinghe, D.; Jaen, J.; Medina, J.; Hungate, R.; Shen, W. Discovery of potent LPA2 (EDG4) antagonists as potential anticancer agents. *Bioorg. Med. Chem. Lett.* **2008**, *18*, 1037–1041.

- (15) Fells, J. I.; Tsukahara, R.; Fujiwara, Y.; Liu, J.; Perygin, D. H.; Osborne, D. A.; Tigyi, G.; Parrill, A. L. Identification of non-lipid LPA3 antagonists by virtual screening. *Bioorg. Med. Chem.* **2008**, *16*, 6207–6217.
- (16) Ohta, H.; Sato, K.; Murata, N.; Damirin, A.; Malchinkhuu, E.; Kon, J.; Kimura, T.; Tobo, M.; Yamazaki, Y.; Watanabe, T.; Yagi, M.; Sato, M.; Suzuki, R.; Murooka, H.; Sakai, T.; Nishitoba, T.; Im, D. S.; Nochi, H.; Tamoto, K.; Tomura, H.; Okajima, F. Ki16425, a subtype-selective antagonist for EDG-family lysophosphatidic acid receptors. *Mol. Pharmacol.* **2003**, *64*, 994–1005.
- (17) Ma, L.; Matsumoto, M.; Xie, W.; Inoue, M.; Ueda, H. Evidence for lysophosphatidic acid 1 receptor signaling in the early phase of neuropathic pain mechanisms in experiments using Ki-16425, a lysophosphatidic acid 1 receptor antagonist. *J. Neurochem.* **2009**, *109*, 603–610.
- (18) González-Gil, I.; Zian, D.; Vázquez-Villa, H.; Hernández-Torres, G.; Martínez, R. F.; Khair-Fernández, N.; Rivera, R.; Kihara, Y.; Devesa, I.; Mathivanan, S.; Del Valle, C. R.; Zambrana-Infantes, E.; Puigdomenech, M.; Cincilla, G.; Sanchez-Martinez, M.; Rodríguez de Fonseca, F.; Ferrer-Montiel, A. V.; Chun, J.; López-Vales, R.; López-Rodríguez, M. L.; Ortega-Gutiérrez, S. A novel agonist of the type 1 lysophosphatidic acid receptor (LPA(1)), UCM-05194, shows efficacy in neuropathic pain amelioration. *J. Med. Chem.* **2020**, *63*, 2372–2390.
- (19) Chrencik, J. E.; Roth, C. B.; Terakado, M.; Kurata, H.; Omi, R.; Kihara, Y.; Warshaviak, D.; Nakade, S.; Asmar-Rovira, G.; Mileni, M.; Mizuno, H.; Griffith, M. T.; Rodgers, C.; Han, G. W.; Velasquez, J.; Chun, J.; Stevens, R. C.; Hanson, M. A. Crystal structure of antagonist bound human lysophosphatidic acid receptor 1. *Cell* **2015**, *161*, 1633–1643.
- (20) Meanwell, N. A. Fluorine and fluorinated motifs in the design and application of bioisosteres for drug design. *J. Med. Chem.* **2018**, *61*, 5822–5880.
- (21) Shinada, N. K.; de Brevern, A. G.; Schmidtke, P. Halogens in protein-ligand binding mechanism: A structural perspective. *J. Med. Chem.* **2019**, *62*, 9341–9356.
- (22) Lassalas, P.; Gay, B.; Lasfargeas, C.; James, M. J.; Tran, V.; Vijayendran, K. G.; Brunden, K. R.; Kozlowski, M. C.; Thomas, C. J.; Smith, A. B., 3rd; Huryn, D. M.; Ballatore, C. Structure property relationships of carboxylic acid isosteres. *J. Med. Chem.* **2016**, *59*, 3183–3203.
- (23) Baksh, M. M.; Kussrow, A. K.; Mileni, M.; Finn, M. G.; Bornhop, D. J. Label-free quantification of membrane-ligand interactions using backscattering interferometry. *Nat. Biotechnol.* **2011**, *29*, 357–360.
- (24) Bornhop, D. J.; Latham, J. C.; Kussrow, A.; Markov, D. A.; Jones, R. D.; Sørensen, H. S. Free-solution, label-free molecular interactions studied by back-scattering interferometry. *Science* **2007**, *317*, 1732–1736.
- (25) Mizuno, H.; Kihara, Y.; Kussrow, A.; Chen, A.; Ray, M.; Rivera, R.; Bornhop, D. J.; Chun, J. Lysophospholipid G protein-coupled receptor binding parameters as determined by backscattering interferometry. *J. Lipid Res.* **2019**, *60*, 212–217.
- (26) Ray, M.; Nagai, K.; Kihara, Y.; Kussrow, A.; Kammer, M. N.; Frantz, A.; Bornhop, D. J.; Chun, J. Unlabeled lysophosphatidic acid receptor binding in free solution as determined by a compensated interferometric reader. *J. Lipid Res.* **2020**, *61*, 1244–1251.
- (27) Whetstone, W. D.; Hsu, J. Y.; Eisenberg, M.; Werb, Z.; Noble-Haeusslein, L. J. Blood-spinal cord barrier after spinal cord injury: relation to revascularization and wound healing. *J. Neurosci. Res.* **2003**, *74*, 227–239.
- (28) Basso, D. M.; Fisher, L. C.; Anderson, A. J.; Jakeman, L. B.; McTigue, D. M.; Popovich, P. G. Basso Mouse Scale for locomotion detects differences in recovery after spinal cord injury in five common mouse strains. *J. Neurotrauma* **2006**, *23*, 635–659.
- (29) Hopper, D. W.; Ragan, S. P.; Hooks, S. B.; Lynch, K. R.; Macdonald, T. L. Structure-activity relationships of lysophosphatidic acid: conformationally restricted backbone mimetics. *J. Med. Chem.* **1999**, *42*, 963–970.
- (30) Bornhop, D. J.; Kammer, M. N.; Kussrow, A.; Flowers, R. A., 2nd; Meiler, J. Origin and prediction of free-solution interaction studies performed label-free. *Proc. Natl. Acad. Sci. U.S.A.* **2016**, *113*, E1595–E1604.
- (31) Kammer, M. N.; Kussrow, A. K.; Bornhop, D. J. Longitudinal pixel averaging for improved compensation in backscattering interferometry. *Opt. Lett.* **2018**, *43*, 482–485.
- (32) Kammer, M. N.; Kussrow, A. K.; Olmsted, I. R.; Bornhop, D. J. A highly compensated interferometer for biochemical analysis. *ACS Sens.* **2018**, *3*, 1546–1552.
- (33) Morris, G. M.; Huey, R.; Lindstrom, W.; Sanner, M. F.; Belew, R. K.; Goodsell, D. S.; Olson, A. J. AutoDock4 and AutoDockTools4: Automated docking with selective receptor flexibility. *J. Comput. Chem.* **2009**, *30*, 2785–2791.
- (34) Biasini, M.; Bienert, S.; Waterhouse, A.; Arnold, K.; Studer, G.; Schmidt, T.; Kiefer, F.; Cassarino, T. G.; Bertoni, M.; Bordoli, L.; Schwede, T. SWISS-MODEL: modelling protein tertiary and quaternary structure using evolutionary information. *Nucleic Acids Res.* **2014**, *42*, W252–W258.
- (35) Dolinsky, T. J.; Czodrowski, P.; Li, H.; Nielsen, J. E.; Jensen, J. H.; Klebe, G.; Baker, N. A. PDB2PQR: expanding and upgrading automated preparation of biomolecular structures for molecular simulations. *Nucleic Acids Res.* **2007**, *35*, W522–525.
- (36) Dolinsky, T. J.; Nielsen, J. E.; McCammon, J. A.; Baker, N. A. PDB2PQR: an automated pipeline for the setup of Poisson-Boltzmann electrostatics calculations. *Nucleic Acids Res.* **2004**, *32*, W665–667.
- (37) Li, H.; Robertson, A. D.; Jensen, J. H. Very fast empirical prediction and rationalization of protein pKa values. *Proteins* **2005**, *61*, 704–721.
- (38) Søndergaard, C. R.; Olsson, M. H.; Rostkowski, M.; Jensen, J. H. Improved treatment of ligands and coupling effects in empirical calculation and rationalization of pKa values. *J. Chem. Theory Comput.* **2011**, *7*, 2284–2295.
- (39) Czodrowski, P.; Dramburg, I.; Sottriffer, C. A.; Klebe, G. Development, validation, and application of adapted PEOE charges to estimate pKa values of functional groups in protein-ligand complexes. *Proteins* **2006**, *65*, 424–437.
- (40) Valentine, W. J.; Fells, J. I.; Perygin, D. H.; Mujahid, S.; Yokoyama, K.; Fujiwara, Y.; Tsukahara, R.; Van Brocklyn, J. R.; Parrill, A. L.; Tigyi, G. Subtype-specific residues involved in ligand activation of the endothelial differentiation gene family lysophosphatidic acid receptors. *J. Biol. Chem.* **2008**, *283*, 12175–12187.
- (41) Marín-Ramos, N. I.; Balabasquer, M.; Ortega-Nogales, F. J.; Torrecillas, I. R.; Gil-Ordóñez, A.; Marcos-Ramiro, B.; Aguilar-Garrido, P.; Cushman, I.; Romero, A.; Medrano, F. J.; Gajate, C.; Mollinedo, F.; Philips, M. R.; Campillo, M.; Gallardo, M.; Martín-Fontecha, M.; López-Rodríguez, M. L.; Ortega-Gutiérrez, S. A potent isoprenylcysteine carboxylmethyltransferase (ICMT) inhibitor improves survival in Ras-driven acute myeloid leukemia. *J. Med. Chem.* **2019**, *62*, 6035–6046.
- (42) Marcos-Ramiro, B.; Gil-Ordóñez, A.; Marín-Ramos, N. I.; Ortega-Nogales, F. J.; Balabasquer, M.; Gonzalo, P.; Khair-Fernández, N.; Rolas, L.; Barkaway, A.; Nourshargh, S.; Andrés, V.; Martín-Fontecha, M.; López-Rodríguez, M. L.; Ortega-Gutiérrez, S. Isoprenylcysteine carboxylmethyltransferase-based therapy for Hutchinson-Gilford progeria syndrome. *ACS Cent. Sci.* **2021**, *7*, 1300–1310.